ChemPubSoc Europe

DOI: 10.1002/open.201900085

Open Access ChemistryOPEN Full Papers

Special Collection

A Benchmark of Density Functional Approximations For Thermochemistry and Kinetics of Hydride Reductions of Cyclohexanones

Xavier Deraet,[a] Tatiana Woller,[a] Ruben Van Lommel,[a, c] Frank De Proft,*[a] Guido Verniest,[b] and Mercedes Alonso*[a]

The performance of density functionals and wavefunction methods for describing the thermodynamics and kinetics of hydride reductions of 2-substituted cyclohexanones has been evaluated for the first time. A variety of exchange correlation functionals ranging from generalized gradient approximations to double hybrids have been tested and their performance to describe the facial selectivity of hydride reductions of cyclohexanones has been carefully assessed relative to the CCSD(T) method. Among the tested methods, an approach in which single-point energy calculations using the double hybrid B2PLYP–D3 functional on ωB97X–D optimized geometries provides the most accurate transition state energies for these kinetically-controlled reactions. Moreover, the role of torsional strain, temperature, solvation, noncovalent interactions on the stereoselectivity of these reductions was elucidated. Our results indicate a prominent role of the substituent on the *cis*/*trans* ratios driven by the delicate interplay between torsional strain and dispersion interactions.

1. Introduction

The nucleophilic addition to a carbonyl functionality, ubiquitous in ketones, aldehydes and carboxylates, is one of the key reactions in organic chemistry allowing the synthesis of a large spectrum of products. In particular, the nucleophilic addition of a hydride to a chiral cycloalkanone induces the formation of a mixture of one or more diastereomers depending on the selectivity of the attack (Figure 1).[1] The relative ratio of axial: equatorial alcohols depends on several parameters, including steric hindrance,[1] stereoelectronic effects,[2] bulkiness of the hydride reagents[3–7] and coordinating ability of the solvent.[3–7]

Due to the importance of the diastereomeric mixture ratio in synthetic pathways, the effects of all these parameters on the reduction of substituted cyclohexanones have been extensively investigated experimentally, resulting into several models to rationalize the more favoured spatial approach of the hydride towards the carbonyl functionality. The most accepted model for describing the approach of a nucleophile towards substituted carbonyls is the Felkin-Anh model (Figure 2).[8] The key idea is to place the largest substituent in terms of steric hindrance (L) orthogonal to the carbonyl moiety, allowing the nucleophile to attack preferentially from the least hindered side,[9] according to the Bürgi-Dunitz angle of 107°.[9] The model was further extended taking into account the electronic factors of the substituents. Electron-withdrawing substituents (EWG) are defined as L-substituents independent of their bulkiness and, accordingly, they are placed perpendicular to the carbonyl moiety.[8c] Such conformation becomes stabilized by hyperconjugation involving the low-lying $\sigma^*_{C_\alpha-L}$ and the π-orbital of the carbonyl group, allowing delocalization of electron density from the reaction centre towards L. As such, the carbonyl moiety becomes more susceptible for the nucleophilic attack. Finally, if the C_α-substituent is a heteroatom amenable to chelation with the counterion of the reducing agent (*e.g.* Mg^{2+}, Zn^{2+}, Al^{3+}, Cu^{2+}), the conformation is locked allowing the

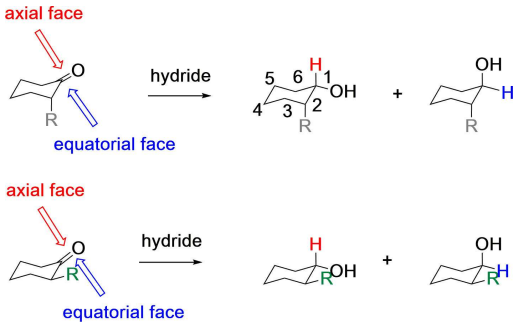

Figure 1. Facial stereoselectivity of the hydride addition to 2-substituted cyclohexanones.

[a] X. Deraet, T. Woller, R. Van Lommel, Prof. F. De Proft, Prof. M. Alonso
Department of General Chemistry (ALGC), Vrije Universiteit Brussel (VUB), Pleinlaan 2, 1050 Elsene, Brussels, Belgium
E-mail: fdeprof@vub.be
mercedes.alonso.giner@vub.be
[b] Prof. G. Verniest
Research group of Organic Chemistry (ORGC), Departments of Bio-engineering Sciences and Chemistry, Vrije Universiteit Brussel (VUB), Pleinlaan 2, 1050 Elsene, Brussels, Belgium
[c] R. Van Lommel
Molecular Design and Synthesis, Department of Chemistry, KU Leuven, Celestijnenlaan 200F Leuven Chem&Tech, box 2404, 3001 Leuven, Belgium

Supporting information for this article is available on the WWW under https://doi.org/10.1002/open.201900085

Special Collection *An invited contribution to a Special Collection dedicated to Computational Chemistry*

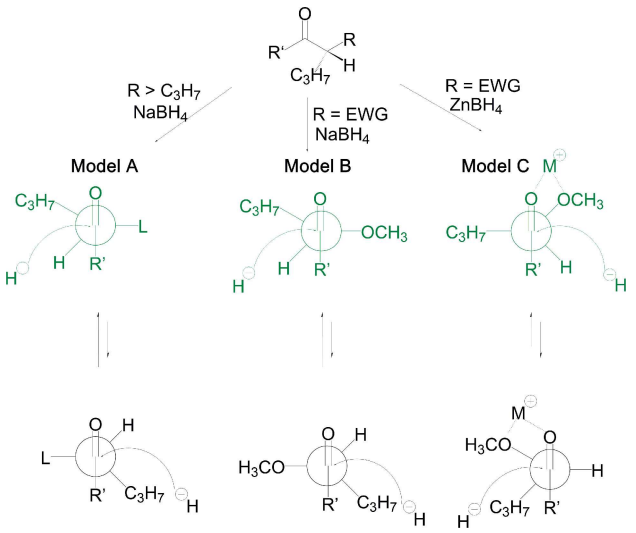

Figure 2. Schematic representation of the Newman projections according to the Felkin-Anh model for bulky substituents (Model A), electron-withdrawing substituents (EWG) without chelation (Model B) and with chelation (Model C).

nucleophile to attack the carbonyl moiety from the least hindered side.[8c]

Nevertheless, Felkin-Anh models assume free rotation around the C–C bond in order to adopt the lowest-energy staggered conformation and therefore, they cannot be directly applied to cycloalkanones. To describe the facial selectivity of cycloalkanone reductions, different models were introduced in which the experimental observations are described in terms of: *(i)* steric hindrance and torsional strain,[8b] *(ii)* asymmetry in π-orbitals,[10] *(iii)* electrostatic repulsion effects[11] or *(iv)* hyperconjugation.[12] The most common approach to predict the stereoselectivity of a nucleophilic attack on cyclohexanones is based on the torsional strain of the transition states. According to this model, the transition state resulting from the equatorial attack of the hydride exhibits more torsional strain than the one corresponding to an axial attack.[8b] An axial face approach of the nucleophile would push the C=O bond away from the other bonds, inducing an energetically more favoured staggered conformation, as represented in Figure 3b.

However, the facial selectivity of the nucleophilic attack is largely influenced by the size of the reducing agent in such a way that small nucleophiles usually add to the axial face, whereas bulky agents preferentially attack the equatorial face (Figure 3a).[13] In the case of small-sized reducing agents, the preferential axial approach seems to be related to the higher stability of the resulting equatorial alcohol relative to the axial product and, hence, the reaction seems to be thermodynamically controlled.[1] By contrast, in the case of bulky reducing reagents, steric hindrance and, more specifically, 1,3-diaxial strain plays an important role by blocking the axial side favouring the equatorial approach of the hydride (Figure 3a).[14] In addition to steric hindrance and torsional strain, asymmetry in the LUMO π* orbital of the carbonyl group was also assumed to determine the final outcome of the nucleophilic addition in cyclohexanones.[10] As schematically shown in Figure 3c, the lobe of the LUMO of the carbonyl carbon atom in substituted cyclohexanones is larger on the axial face than on the equatorial side.[15] Consequently, the largest stabilizing interaction with the HOMO of the nucleophile is expected for the axial approach.[10]

Next, the selectivity of the nucleophilic attack can be further described in terms of electrostatic effects,[11] when electron-withdrawing groups are located at C_4. When these groups are located at axial positions, a noticeable increase for the equatorial alcohol is observed as compared to cyclohexanones without electron-withdrawing substituents.[11] A plausible explanation for these experimental findings relies on electrostatic effects (Figure 3d) since the equatorial attack by the nucleophile is largely destabilized by electrostatic repulsion with the axial EWG substituent.[11] By contrast, the axial attack is favoured by attractive electrostatic interactions, explaining the enhanced ratio for the equatorial alcohol.[11]

An alternative model based on the stabilization of the transition state by antiperiplanar allylic bonds was introduced by Cieplak.[12] According to this model, the hyperconjugation of the forming $\sigma^*_{C\text{-}H}$ orbital with the geometrically aligned antiperiplanar σ orbitals controls the stereoselectivity of nucleophilic additions to cyclohexanones (Figure 3e). In the transition state of an equatorial addition, the two antiperiplanar C–C bonds to the incipient C–H bond donates electron density to the $\sigma^*_{C\text{–}H}$ orbital. However, in the axial approach, the neighbouring axial C–H bonds are antiperiplanar to the forming

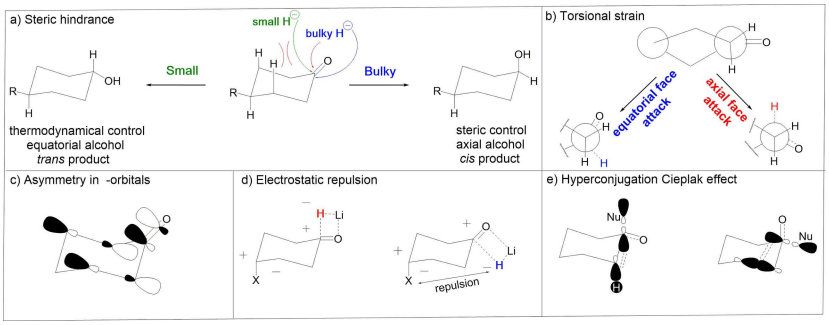

Figure 3. Representation of the different models to describe the stereoselectivity of the hydride reductions on cyclohexanones.

C–H bond. Since the C–H bonds are postulated to be better electron donors than C–C bonds, the incipient σ^*_{C-H} orbital gets stabilized in a larger extent by hyperconjugation in the axial approach and, accordingly, the axial addition is favoured.[16] Although this model was successful in explaining the stereoselectivity of a variety of substituent effects,[17] criticisms on this model have been put forward.[18]

A powerful tool to elucidate the importance of the different factors controlling the high stereoselectivity of hydride reductions of cyclic ketones relies on quantum chemistry. Indeed, the reaction mechanism of the hydride reductions in cyclohexanones has been extensively investigated through computational methods, principally by the group of Houk.[11,13,19] Overall, the quantum chemical studies support the Felkin-Anh torsional strain model,[19a,b,e] although additional factors including steric effects, substrate conformation and nucleophile bulkiness also affect the stereoselectivity of such reactions.[19c–d] So far, most of the computational studies dealing with hydride reductions of cyclic ketones were performed using density functional theory (DFT) methods, in particular with the popular B3LYP[20] hybrid functional.[19c–e] Only recently, the reduction of several cyclic ketones was also investigated with the M06-2X[21a] hybrid functional, but better agreement with experimental results was observed for B3LYP.[13] Nevertheless, recent benchmark results on wavefunction and DFT methods have shown that the B3LYP functional often performs worse as compared to other hybrid functionals for general main group thermochemistry and kinetics, discouraging its usage as standard method.[22] The main shortcomings of the popular B3LYP density functional are the following: (*i*) systematic underestimation of reaction barrier heights, (*ii*) inability to treat London dispersion interactions and (*iii*) it fails for transition-metal containing structures.[23]

Since no benchmark studies are reported to date for hydride reductions of cyclohexanones, we decided to assess for the first time the performance of a variety of density functionals to describe the barrier heights and reaction energies of such important reactions. For our benchmark, a set of 2-substituted cyclohexanones bearing different substituents (Me, OMe, SMe and Cl) and a prototypical reducing agent ($LiAlH_4$) were considered (Figure 4). These cyclohexanones were selected due to the different stereoelectronic effects of the substituents and the commercial availability of the 2-substituted cyclohexanones.[19d–e,24] The selected density functionals span

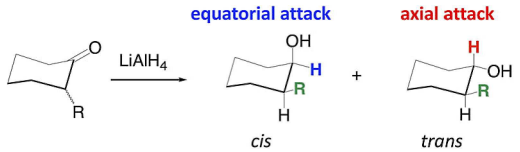

	cis	trans
R = Me (**1**)	11%	89%
R = OMe (**2**)	n.a.	n.a.
R = SMe (**3**)	79%	21%
R = Cl (**4**)	83%	17%

Figure 4. Set of 2-substituted cyclohexanones considered in the benchmark study together with experimentally determined *cis*:*trans* ratios at −78 °C. The experimental procedure can be found in the supporting information.

from generalized gradient approximations to double hybrid functionals. More specifically, several Minnesota-class of hybrid functionals (M06, M06-2X and M11) have been tested due to their high accuracy for main-group thermochemistry and kinetics.[21] Besides, the ωB97X–D functional, which separates the exchange energy into long-range and short-range contributions and accounts for dispersion corrections, was also included.[25] This range-separated hybrid functional emerges as one of the most promising functionals to describe the geometry and thermochemistry of organic reactions as well as transition metal compounds.[26] Finally, the performance of double-hybrid functionals,[27] including a certain amount of HF exchange and MP2 electron correlation, together with the Møller-Plesset MP2[28] method were also investigated. Our main goal is to assess the performance of a variety of contemporary DFT and double-hybrid DFT methods to describe the thermochemistry and kinetics of hydride reductions of substituted cyclohexanones. Moreover, our findings provide new insights into the different stereoelectronic factors governing the facial selectivity of such key reactions. Our calculations indicate that the torsional strain of the transition state is not the main factor controlling the stereoselectivity of 2-cyclohexanones bearing electron-withdrawing substituents.

2. Computational Methodology

The performance of seven popular DFT exchange-correlation functionals and the MP2 approach has been investigated by comparison with the gold-standard in quantum chemistry, CCSD(T).[29] As introduced by Perdew, exchange-correlation functionals can be organized into five rungs of Jacob's Ladder of DFT.[30] The first rung is the local spin-density approximation[31] (LSDA), which is exact for an infinite uniform electron gas in which the electron density is constant over space, but highly inaccurate for molecular systems with inhomogeneous density distribution.[32,33] In order to account for inhomogeneities in the electron density, a second rung of functionals was introduced consisting of generalized gradient approximation (GGA) functionals.[34] The GGA functionals (e.g. PBE[35]) depend on the electron density and its gradient, whereby the correct behaviour of the density over space is described. Due to the general improved performance of GGA functionals over the LSDA approach,[35–37] meta-GGA functionals depending on higher order derivatives of the electron density were developed and classified into the third rung.[38,39] The fourth rung of Jacob's Ladder is occupied by hybrid functionals, like B3LYP,[20] M06,[21a] M06-2X,[21a] M11[40] and ωB97X–D,[25] which are characterized by a varying amount of exact Hartree-Fock exchange. The final fifth rung is composed of double-hybrid functionals, such as B2PLYP,[27a] containing an exact amount of Hartree-Fock exchange as well as a given percentage of exact electron-correlation.

Density functional calculations were carried out with the Gaussian 09.D01 software package.[41] First, the stationary points were fully optimized and characterized by harmonic-vibrational-frequency calculations using the cc-pVDZ Dunning basis set[42] in combination with several density functionals: PBE–D3, B3LYP–D3, M06-2X, M06, ωB97X–D and M11. PBE and B3LYP calculations were performed including Grimme's DFT–D3 empirical dispersion with the Becke-Johnson damping function to overcome the deficiencies of conventional functionals in the treatment of dispersion.[43] The DFT–D3 empirical dispersion correction improves the accuracy not only for noncovalent interactions, but also for reaction barrier heights.[44]

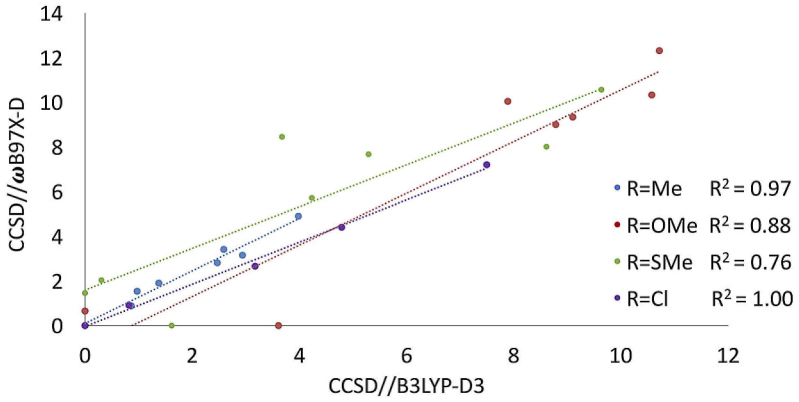

Figure 5. Relationship between the CCSD relative energies (kcal mol^{-1}) of the eight transition states evaluated on ωB97X–D and B3LYP–D3 optimized geometries for the reduction of different 2-substituted cyclohexanones (**1**--**4**) by $LiAlH_4$.

The nature of the stationary points was assessed according to the appropriate number of negative eigenvalues of the Hessian matrix from the frequency calculations. Minima are characterized by positive eigenvalues, whereas transition states exhibit one negative eigenvalue corresponding to the hydride transfer. The thermodynamic contributions to the enthalpy (ΔH) and Gibbs free energy (ΔG) were computed at 1 atm for 298 K and 195 K. In order to evaluate more accurate electronic energies, subsequent single-point calculations were performed at the DFT/aug-cc-pVTZ[44] level of theory. For all the DFT calculations, the large "ultrafine" grid was used to minimize the integration grid errors, especially important for the Minnesota functionals.[45] Single-point energy calculations were also performed with the double-hybrid B2PLYP functional[27a] adding the D3 dispersion correction, as well as with the MP2 method. These single-point energy calculations were performed on both ωB97X–D and B3LYP–D3-optimized geometries. To assess the performance of the DFT functionals and the MP2 approach, single-point energy calculations were carried out with the CCSD[46] and CCSD(T)[29] method in combination with the cc-pVTZ basis set with the Molpro2012 software.[47] To evaluate the influence of the geometry on the reference energies, the CCSD calculations were performed on both the ωB97X–D and B3LYP–D3-optimized geometries (Figure 5). Interestingly, the CCSD relative energies computed on the different optimized geometries are almost linearly correlated and the energy differences are lower than 1 kcal mol^{-1} for all substituents, suggesting that the influence of the level of theory on geometry optimization is rather small. Based on these findings, the costly CCSD(T) calculations were only performed on the ωB97X–D-optimized geometries.

The accuracy of the different computational methods to describe the transition state energies as well as the conformational preferences of 2-substituted cyclohexanones and cyclohexanols was assessed by means of the mean unsigned error (MUE) and the root-mean-square deviation (RMSD) relative to the CCSD(T)/cc-pVTZ energies:

$$MUE = \frac{1}{N}\sum_{i=1}^{N} |x_i - x_{reference}| \quad (1)$$

$$RMSD = \sqrt{\frac{1}{N}\sum_{i=1}^{N} (x_i - x_{reference})^2} \quad (2)$$

Having assessed the performance of different computational methods on the energetic profiles, we then proceeded to scrutinize the different interconversion pathways for the hydride reduction of the different cyclohexanones. Besides the transition states, the lowest energy coordination pre-reactive and post-reactive complexes were also optimized at the ωB97X–D/cc-pVDZ level of theory. Subsequent, single-point energy calculations were performed at the B2PLYP–D3/aug-cc-pVTZ level, since it was proven to provide transition state energies within chemical accuracy. Implicit solvent effects were computed using the polarizable continuum model with radii and nonelectrostatic terms from Truhlar and coworkers' SMD model[48] at the B2PLYP–D3/aug-cc-pVTZ level of theory. The solvent effects were calculated at the gas-phase geometries, resulting in a solvation free energy.

To assess the role of the noncovalent interactions on the stereoselectivity, the noncovalent interaction (NCI) index was computed with the NCIPLOT program[49] starting from the B2PLYP–D3 wavefunctions of the optimized geometries. NCI is a semi-quantitative method that characterizes noncovalent interactions according to the electron density[50] and the reduced density gradient (s):

$$s = \frac{1}{2(3\pi^2)^{1/3}} \frac{|\nabla\rho|}{\rho^{3/4}} \quad (3)$$

The NCI index identifies covalent and noncovalent interactions by plotting the reduced density gradient against the product of the electron density and the sign of second eigenvalue λ_2 of the electron-density Hessian matrix. Noncovalent interactions are determined by the presence of spikes at low density values due to the annihilation of the reduced density gradient at these points. Based on this method, the strength of the interaction is derived from the density values of the low-gradient spikes. Dispersion interactions usually appear at very low-density values ($\rho > 0.01$ a.u.), whereas stronger hydrogen bonds appear at higher density values ($0.01 < \rho < 0.05$ a.u.). Attractive interactions, such as a hydrogen bonding, are characterized by negative λ_2, whereas positive λ_2 corresponds to repulsive interactions, like steric clashes. Since the sign of the second eigenvalue [sign(λ_2)] is indicative for the type of interaction, the gradient is plotted against the product of the sign (λ_2) and the electron density function.

Density properties can be integrated within the NCI region to obtain the volume (V_{NCI}) of the isosurface enclosed within it.[51]

$$V_{NCI} = \int_{\Omega_{NCI}} d\vec{r} \quad (4)$$

To perform such integrations, it is necessary to establish a unique definition of the NCI region. To identify this region, the $s(\rho)$ plot of the nonsubstituted cyclohexanone was computed. The lower edge of the reference $s(\rho)$ curve is splined and all the points of the 2-substituted cyclohexanones $s(\rho)$ plot lying below the splined curve are localized in real space. In practice, these integrations are performed numerically, by summation over a cubic grid with 0.1 a.u. increments. It is also possible to separate the attractive and repulsive contributions depending on the sign of the second eigenvalue (λ_2) at each point.

A very important tool is the visualization of the gradient isosurface in real space. The reduced gradient isosurface can be conveniently visualized using the VMD program[52] and coloured according to the value of the sign(λ_2)ρ. A RGB (red-blue-green) scale is typically employed: red isosurfaces indicate repulsive interactions, blue stands for attractive interactions, and green for very weak van der Waals-type interactions. Importantly, NCI is very stable with respect to the computational method, providing similar NCI quantities regardless of the method and the basis set.[53] From these calculations, further insight into the facial selectivity of hydride reductions in 2-substituted cyclohexanones was attained.

3. Results and Discussion

3.1. Benchmark Study of Density Functional Methods for Thermochemistry and Kinetics of Hydride Reductions of Cyclohexanones

The performance of the different functionals was assessed on a set of experimentally well-characterized hydride reduction reactions, involving 2-methyl (**1**), 2-methoxy (**2**), 2-methylthio (**3**), 2-chlorocyclohexanone (**4**) and $LiAlH_4$ (Figure 4). Besides the ease to generate adequate experimental data, these systems are advantageous since high-level correlation methods calculations are affordable. Two main mechanisms are proposed for such nucleophilic additions (Figure 6). In the first mechanism,[1] the first step involves the addition of $LiAlH_4$ to the axial or equatorial face of the cyclohexanone. This rate-determining step (RDS) is characterized by an important interaction between the HOMO orbital of the incoming nucleophile and LUMO of the carbonyl functionality, resulting into the formation of a new σ-bond between the nucleophile and the carbon atom of the carbonyl functionality together with the corresponding destruction of the carbonyl π-bond. In a second step, the negatively charged oxygen atom is protonated resulting into the alcohol

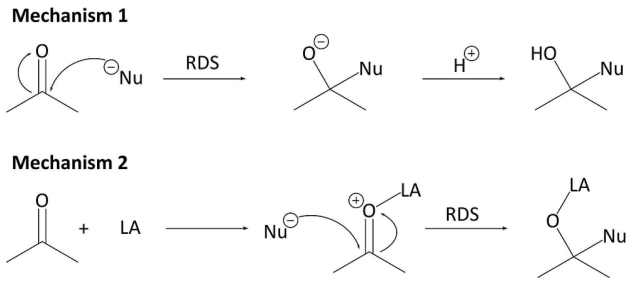

Figure 6. Schematic representation of the two-step mechanisms describing the nucleophilic addition to a carbonyl functionality.

functionality. In the second mechanism,[1] a Lewis acid (LA) first coordinates the carbonyl oxygen atom resulting in a strong activation. As such, the carbonyl functionality is more prone to the nucleophilic attack, which occurs in a second step determining the rate of the reaction. The first mechanism applies to reactions in which strong nucleophiles are added under basic conditions, while the latter mechanism is postulated for weaker nucleophiles under acidic conditions. Since reducing agents such as $LiAlH_4$ are known to exhibit strong nucleophilic character,[3] we exclusively considered the first mechanism in our research. Furthermore, previous computational studies have shown that the energy profiles related to the cyclohexanone reduction by $LiAlH_4$ involves the early formation of a complex between the reducing agent and the carbonyl functionality and, consequently, a reactant-like transition state is expected.[20]

Based on previous computational studies,[19c–e] eight transition structures need to be considered for describing accurately the facial selectivity of hydride additions on cyclohexanones (Figure 7). On one side, two conformational isomers are available for 2-substituted cyclohexanones corresponding to an equatorial and axial substitution pattern. On the other side, two stable $LiAlH_4$ ground-state isomers are plausible corresponding to a bidentate and a tridentate structure, in which lithium is coordinated to two hydrogen atoms and three hydrogen atoms, respectively.[19c] The various TS structures for the reduction of 2-substituted cyclohexanones are shown in Figure 7. The structures **a**–**d** are referred to as bidentate, whereas the structures **a'**--**d'** are tridentate. In the next sections, the performance of the different functionals to assess the relative energies of reactants, transition states and products is carefully investigated.

3.2 Conformations of Starting Reactants: 2-Substituted Cyclohexanones

Table S1 in the supporting information collects the relative energies of the axial and equatorial chair conformations for 2-methyl (**1**), 2-methoxy (**2**), 2-methylthio (**3**) and 2-chlorocyclohexanone (**4**) computed with the different electronic structure methods together with the mean unsigned error (MUE) and root-mean-square deviation (RMSD). The statistical deviations were evaluated relative to CCSD(T)/cc-pVTZ//ωB97X–D/cc-pVDZ reference data and can be visualized in Figure 9. The reference relative energies of the axial and equatorial conformations are summarized in Figure 8, together with those provided by the overall best performing functional.

Regardless of the substituent, none of the computational methods yield a statistical deviation greater than 1 kcal mol^{-1} with respect to the reference CCSD(T) method. Importantly, nearly all the methods provide the same global minima conformation corresponding to the equatorial conformer for 2-methylcyclohexanone (**1**) and the axial conformation for the cyclohexanones **2**–**4**.

From Figure 9, it becomes clear that the performance of the DFT and wavefunction methods depends on the substituent.

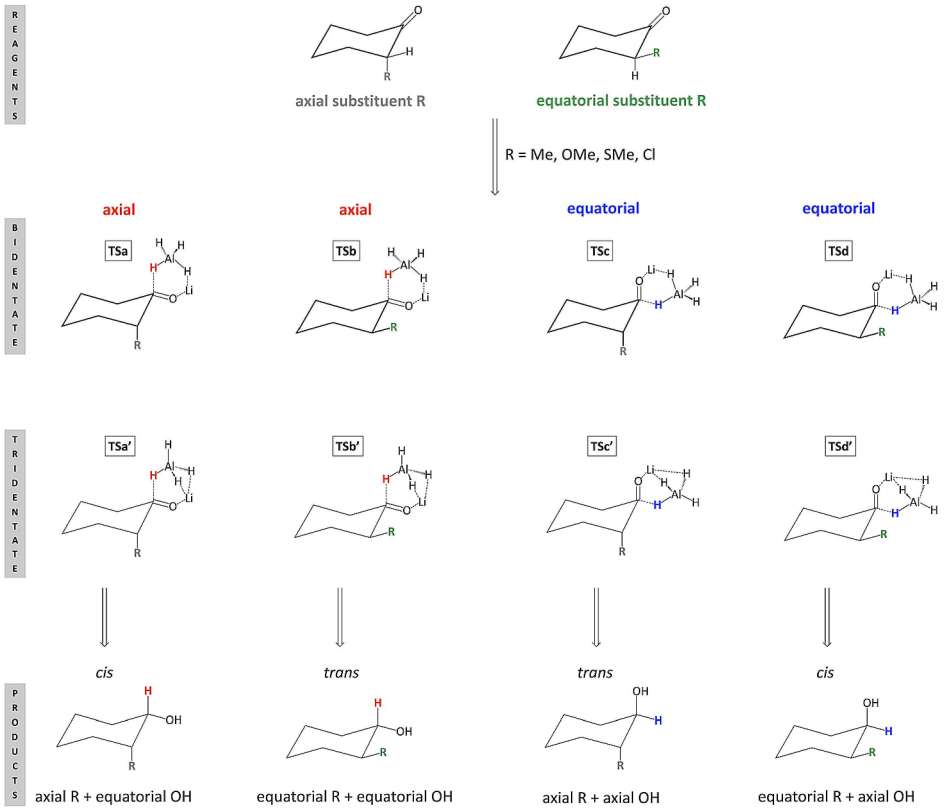

Figure 7. Representation of the transition states and the corresponding alcohol products involved in the reduction of 2-substituted cyclohexanones by $LiAlH_4$. The TS structures **a–d** correspond to bidentate arrangements, while structures **a′-d′** are tridentate transition states.

R = Me	E_{rel} = 1.87 (1.92)	E_{rel} = 0.00 (0.00)
R = OMe	E_{rel} = 0.00 (0.00)	E_{rel} = 1.78 (1.47)
R = SMe	E_{rel} = 0.00 (0.00)	E_{rel} = 0.33 (0.46)
R = Cl	E_{rel} = 0.00 (0.00)	E_{rel} = 1.35 (1.15)

Figure 8. CCSD(T) relative energies for the axial and equatorial chair conformations of the different 2-substituted cyclohexanones (**1**–**4**). The relative energies between brackets correspond to M06-2X, the best performing functional over this set.

Largest RMSD and MUE values are obtained for the methoxy substituent. In this case, a larger variation in performance is observed for functionals belonging to the same rung of Jacob's ladder as compared with the other substituents. Among hybrid functionals, the M11 functional with a variable amount of HF exchange[54] performs the best (MUE = 0.11 kcal mol^{-1}), followed by the M06-2X functional (MUE = 0.16 kcal mol^{-1}) and the B3LYP–D3 functional (MUE = 0.22 kcal mol^{-1}). However, the accuracy of M06 is significantly worse by a factor of 6 (MUE = 0.64 kcal mol^{-1}). Also, a large variability in performance is observed for range-separated hybrid functionals: M11 and ωB97X–D. The MUE associated with the ωB97X–D functional (MUE = 0.40 kcal mol^{-1}) is four times larger than the MUE of M11. Finally, single-point energy calculations using the double-hybrid functional B2PLYP–D3 and MP2 yield to less accurate relative conformational energies for the cyclohexanone moiety relative to the CCSD(T) method.

For 2-methylcyclohexanone (**1**), the hybrid M11 and M06-2X, the PBE functional and B2PLYP–D3 provide a similar accuracy than CCSD(T) with MUE values lower than 0.05 kcal mol^{-1}. Slightly larger deviations are found for the hybrid functionals ωB97X–D, B3LYP–D3 and M06. Among the tested methods, the MP2 approach is clearly the worst-performing one, regardless of the optimized geometry. Similar perform-

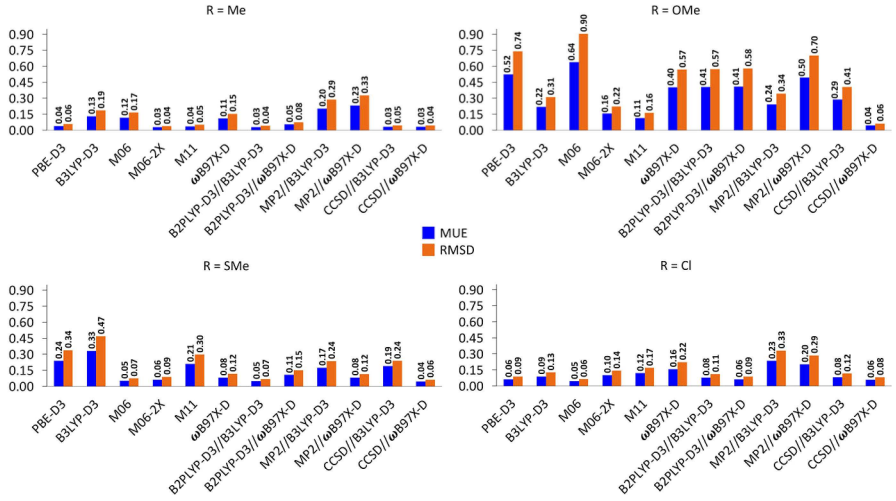

Figure 9. MUE and RMSD (in kcal mol^{-1}) relative to CCSD(T) for describing the axial:equatorial energies of the starting cyclohexanones (**1**–**4**) bearing different substituents.

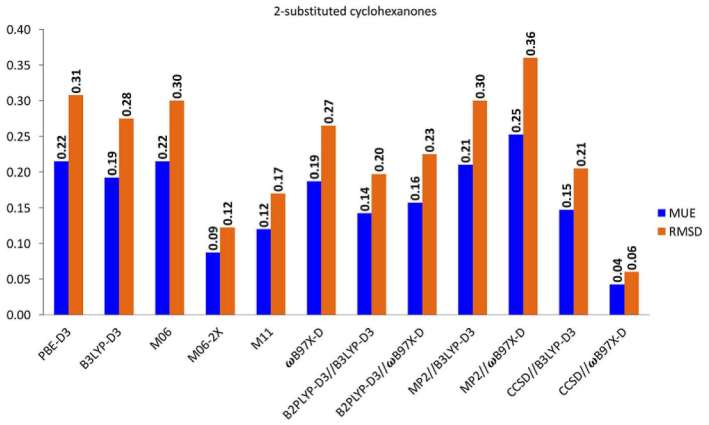

Figure 10. Average MUE and RMSD (in kcal mol^{-1}) for describing the axial:equatorial relative energies for the starting cyclohexanones (**1**–**4**).

ances are found for the 2-chlorocyclohexanone (**4**) with B2PLYP–D3 and PBE–D3 performing remarkably well. In the case of 2-methylthiocyclohexanone (**3**), the Minnesota functionals M06 and M06-2X together with the double hybrid functional B2PLYP–D3 show the best performance in describing the relative energies of the axial and equatorial conformations with MUE values of about 0.05 kcal mol^{-1}. For such a substituent, the widely used functional B3LYP shows an increased MUE value of 0.33 kcal mol^{-1}. Interestingly, B2PLYP–D3 single-point calculations on the B3LYP-optimized geometries largely reduces the MUE values to 0.05 kcal mol^{-1}.

Figure 10 shows the average MUE and RMSD for the different methods over the complete benchmark set of 2-substituted cyclohexanones (**1**–**4**). Overall, the M06-2X functional with 54% of exact HF exchange outperforms other density functionals and the MP2 method in describing the relative stability of axial:equatorial conformers for the starting reactants. Regarding range-separated hybrid functionals, M11 provides lower statistical error than ωB97X–D for this set of organic compounds. Among the wavefunction methods, MP2 provides relative energies in bad agreement with the CCSD(T) method irrespective of the level of theory used in geometry optimization. The errors linked to CCSD are rather negligible, especially when combined with the ωB97X–D optimized geometries. An alternative to the expensive CCSD calculations involves B2PLYP–D3 single-point energy calculations on lower rung optimized structures, which reduces the MUE and RMSD values. Importantly, the influence of the optimized geometry is rather small for the double hybrid functional and CCSD method.

3.3. $LiAlH_4$ Reduction of 2-Substituted Cyclohexanones

As stated by Luibrand and co-workers,[19c] the reduction towards the final alcohol can occur via eight different transition states in which lithium is coordinated to one (bidentate) or two hydrogen atoms (tridentate), as indicated in Figure 7. Accordingly, eight TSs were fully optimized and characterized for each 2-substituted cyclohexanone (R=CH_3, OCH_3, SCH_3, Cl) at different levels of theory and the corresponding relative energies are

collected in Table S2 together with the MUE and RMSD values relative to CCSD(T) energies. The optimized geometries of the different stationary points at the ωB97X–D/cc-pVDZ level of theory are shown in Figure 11. For solvent based calculations, a more realistic model would consist of the lithium counterion being coordinated with solvent molecules. However, previous computational work has indicated that non-solvated models are sufficient to accurately reproduce experimentally obtained selectivity of hydride reductions.[13,19]

To assess the performance of the DFT functionals and wavefunction methods to predict the relative energy of the eight transition states involved in the reduction of 2-substituted cyclohexanones, the MUE and RMSD were computed relative to CCSD(T) energies (Figure 12). Immediately, it becomes clear that the errors become larger for the description of transition states as compared with the starting cyclohexanones. This is expected since metallic species are only present in the transition structures and, additionally, a high number of structures is considered. Similarly, the performance of the methods depends on the substituents, with the OMe group showing the largest RMSD and MUE values.

In the case of 2-methylcyclohexanone (**1**), most of the functionals, including PBE, M06, M06-2X, M11 and ωB97X–D predict the tridentate **TSb'** as the lowest-energy transition structure, which corresponds to an axial attack by the $LiAlH_4$ with the methyl group in an equatorial position. For these functionals, the MUE and RMSD are within the range of chemical accuracy. By contrast, B3LYP–D3 and MP2 predicts the bidentate structure **TSb** as the most stable transition state. Both **TSb** and **TSb'** lead to the formation of the *trans* alcohol, in good agreement with the experimental data.[24a–b] Among the DFT methods, M11 provides results with the highest accuracy (MUE = 0.44 kcal mol^{-1}). Again, MP2 is the worst performing method, especially when combined with B3LYP-optimized geometries. For the methyl substituent, B2PLYP–D3 single-point energy calculations on lower rung optimized geometries do not improve the performance of exchange-correlation functionals, while increasing the CPU time.

However, for cyclohexanone **2** bearing a methoxy group, M11 predicts **TSb** as the lowest-energy transition structure, whereas the rest of the methods identified **TSd** and **TSd'** as the favoured transition states. At the CCSD(T) level of theory, both transition structures are isoenergetic. Accordingly, hydride addition from the equatorial face of 2-methoxycyclohexanone is favoured, leading to the *cis* alcohol. For the OMe group, only B3LYP–D3 and B2PLYP–D3 provides MUE values lower than 0.6 kcal mol^{-1}. All the heavily parametrized Minnesota hybrid functionals led to larger MUE and RMSD values. Contrary to **1**, B2PLYP–D3 single-point energy calculations on ωB97X–D optimized geometries have a highly positive influence on the description of the transition states energies, reducing the MUE by a factor of 4.

For the SMe group, the double hybrid functional B2PLYP–D3 provides the lowest statistical errors relative to CCSD(T), regardless of the optimized geometry. All hybrid functionals provide MUE values larger than 1 kcal mol^{-1}. It is important to note that different lowest-energy transition structures are found by the different methods. According to the CCSD(T) and B2PLYP electronic energies, **TSb** and **TSd** are almost isoenergetic both having the SMe group in an equatorial position. While **TSb** lead to the formation of a *trans* alcohol, **TSd** provides the *cis* alcohol which is in better agreement with the experimental *cis*:*trans* ratio of 79:21. Only B3LYP–D3, M06, MP2 and B2LYP–D3 electronic energies point out **TSd** as the most favoured transition state. Notwithstanding that entropic factors were not considered in the benchmark, these results already emphasize the importance of the electronic structure method in describing the facial selectivities of the hydride reduction of 2-substituted cyclohexanones, especially for EWG such as OMe and SMe.

In the case of 2-chlorocyclohexanone (**4**), all the methods provide MUE and RMSD values in the range of chemical accuracy. Importantly, nearly all methods pointed the bidentate **TSb** as the lowest-energy transition state which leads to a *trans* alcohol. Similar performances for the different functionals are found for the reduction of 2-methyl (**1**) and 2-chloro (**4**) cyclohexanones. For instance, no striking differences between the PBE–D3 functional and hybrid functionals are observed. M11 is the best-performing hybrid functional with a MUE = 0.41 kcal mol^{-1}, while MP2 performs the worst.

The average MUE and RMSD values, considering all the transition structures ($n = 29$) for the reduction of the differently-substituted cyclohexanones, are plotted in Figure 13. From this graph, it can be inferred that B2PLYP–D3 combined with ωB97X–D optimized geometries provides the lowest MUE and RMSD values over the complete benchmark set. Regardless of the geometry, the double hybrid functional seems more accurate than CCSD and MP2. In order to reassess the good performance of double hybrid functionals, a set of single-point energy calculations on ωB97X–D optimized transition state geometries was also performed with the DSD-PBEP86-D3BJ,[55] a spin-component-scaled double hybrid functional approaching the accuracy of more demanding composite *ab-initio* methods.[55b] As can be inferred from Table S2 and Figure S1, the performance for both hybrid functionals are very similar with MUE values of 0.54 kcal mol^{-1} and 0.47 kcal mol^{-1} for B2PLYP–D3 and DSD-PBEP86-D3BJ, respectively. Therefore, we conclude that double hybrid functionals are clearly the most suitable approach to investigate the barrier heights of hydride reductions. Among the hybrid functionals, B3LYP–D3 is the one that better approaches the relative stability of the different transition structures to CCSD(T). The percentage of exact HF exchange plays an important role, in such a way that the lower this percentage the lower the MUE and RMSD. As such, M06-2X with 54% of nonlocal exchange performs particularly worse for the transition structures, which is expected considering that this functional is parametrized only for nonmetals.[21a] The range-separated hybrid functional ωB97X–D is slightly more accurate than M11, but they perform worse than B3LYP–D3. Both range-separated functionals contain the same amount of long-range contribution (100%), but differ in the amount of short-range HF exchange (ωB97X–D: 22% vs M11: 42.8%).[25,40] Again, the lower amount of nonlocal exchange in the short-range in ωB97X–D provides reduced MUE and RMSD values as compared to M11.

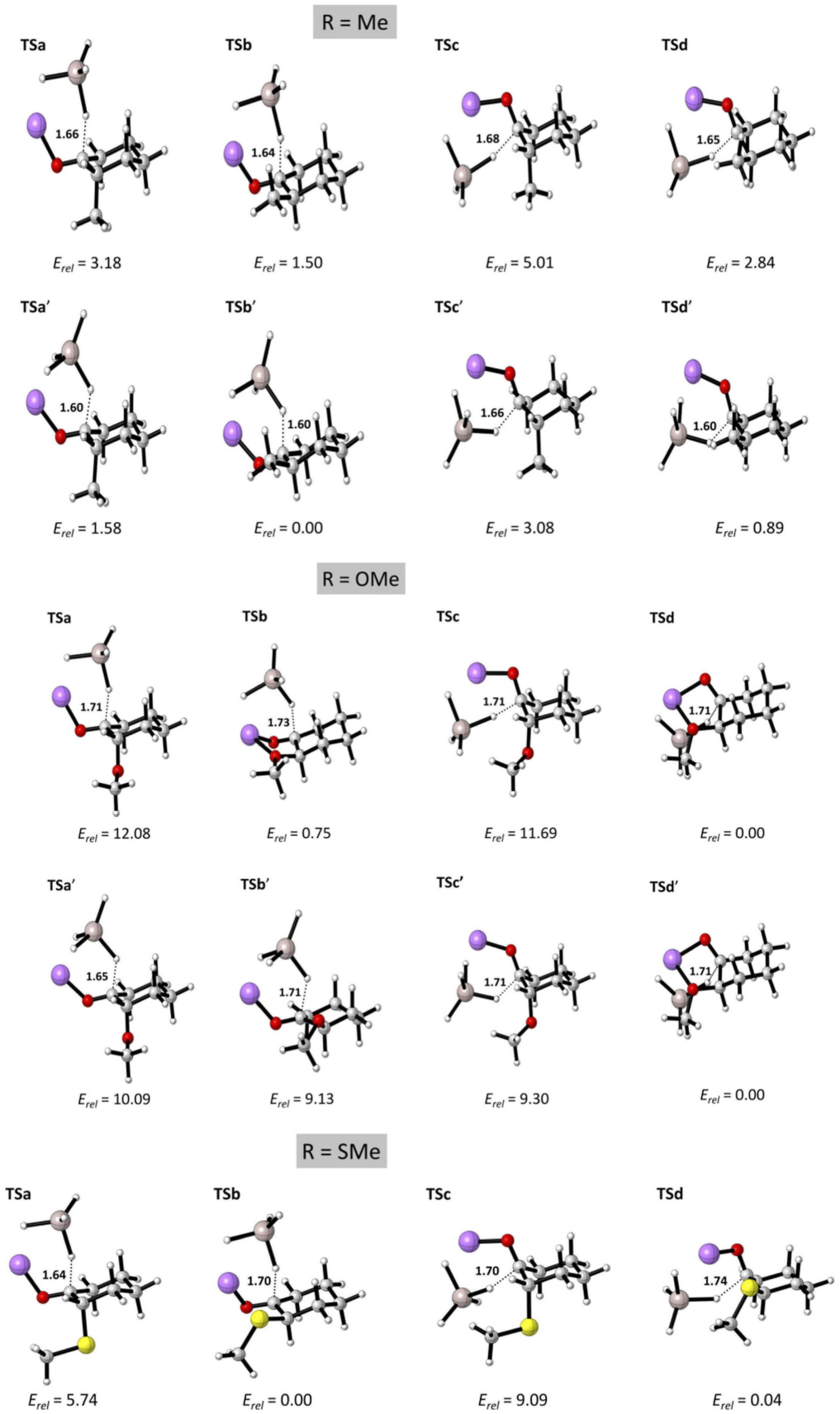

Figure 11. ωB97X–D-optimized geometries of the different transition states for the reduction of each 2-substituted cyclohexanones (**1**–**4**) by $LiAlH_4$. The reference CCSD(T) relative energies (in kcal mol^{-1}) together with the bond length (in Å) of the incipient bond are also shown. For R=Cl, the optimization of **TSa**, **TSb'** and **TSd'** led to a different structure.

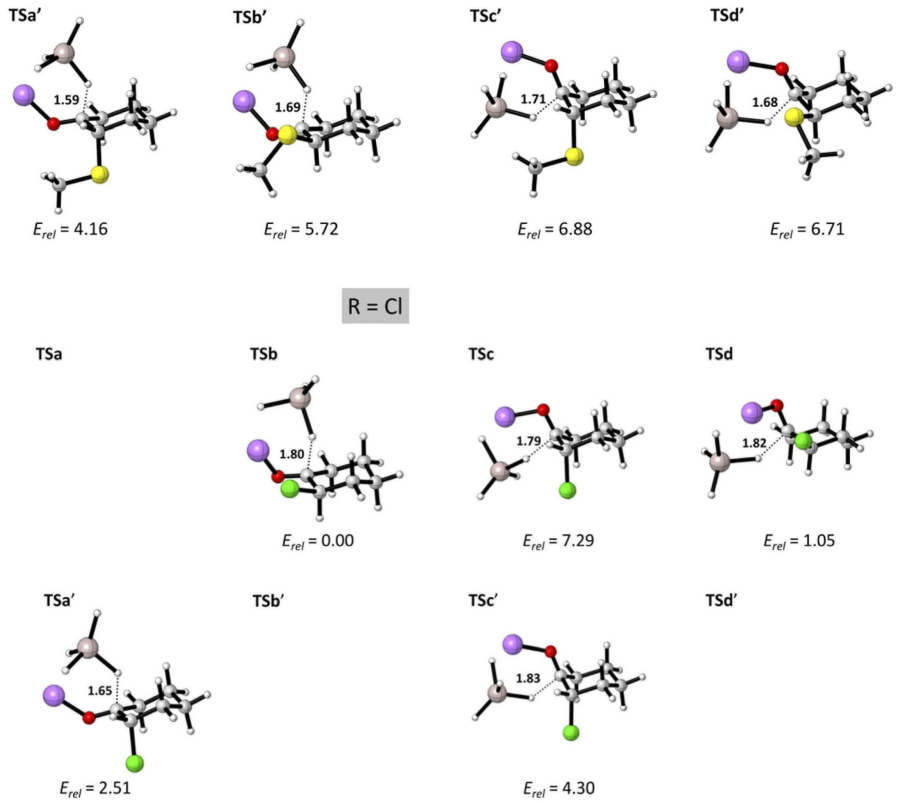

Figure 11. cont.

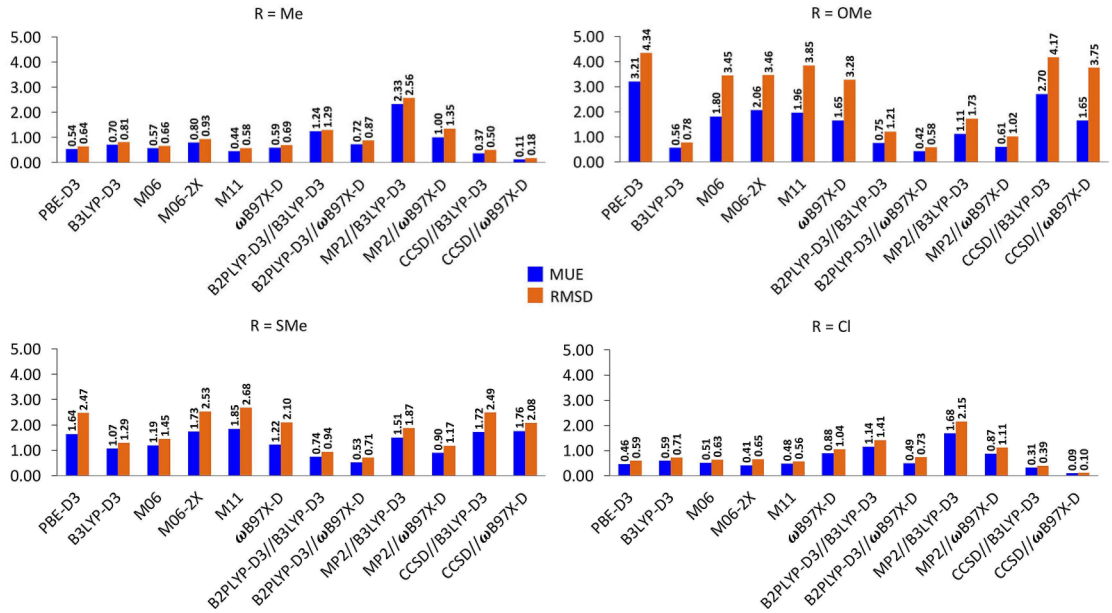

Figure 12. MUE and RMSD (in kcal mol^{-1}) relative to CCSD(T) for describing the transition states energies of the reduction of 2-substituted cyclohexanones (**1**–**4**) by $LiAlH_4$.

Finally, MP2 seems to be the worst method for describing the kinetics of hydride reductions of cyclohexanones. Furthermore, the effect of the geometry in the relative energies is significantly more pronounced in MP2 than in CCSD and B2PLYP–D3 calculations.

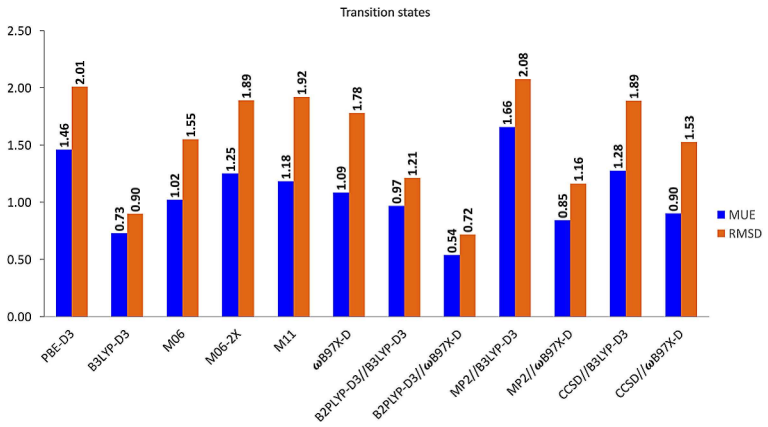

Figure 13. Average MUE and RMSD (in kcal mol^{-1}) for describing the transition state energies of the hydride reduction of 2-substituted cyclohexanones (**1**–**4**).

3.4. Conformations of Final Products: 2-Substituted Cyclohexanols

The relative energies of the 4 different isomers of 2-methyl (**1**), 2-methoxy (**2**), 2-methylthio (**3**) and 2-chlorocyclohexanol (**4**) together with their statistical deviations evaluated with respect to CCSD(T)/cc-pVTZ//ωB97X–D/cc-pVDZ reference data are collected in Table S3. The optimized geometries of the four possible alcohol isomers together with their CCSD(T) and M06 (the overall best performing functional) relative energies are summarized in Figure 14.

In the case of 2-methylcyclohexanol, the *trans* isomer with both substituents in equatorial position is found as the thermodynamically favoured product regardless of the method, in good agreement with the experimental *cis*:*trans* ratio of 11:89 (Figure 4). Nevertheless, the performance of the different methods, with respect to the CCSD(T) data, for predicting the relative energies of the different cyclohexanol isomers is dissimilar, as can be inferred from Figure 15. MP2 provides increased MUE and RMSD values by a factor 3 and 8 as compared to B3LYP–D3 (MUE = 0.30 kcal mol^{-1}) and ωB97X–D (MUE = 0.21 kcal mol^{-1}), respectively. Within the different DFT functionals, it can be observed that unlike the conformers of 2-methylcyclohexanone all hybrid functionals perform much better as compared to PBE. The best performing functional is M11 (MUE = 0.17 kcal mol^{-1}), followed by the range-separated ωB97X–D functional. B2PLYP–D3 single-point calculations on lower-rung optimized geometries appears to have a negative influence on the relative energies of the isolated products, as an increase in MUE-value by a factor 1.9 and 2.6 is observed with respect to B3LYP–D3 and ωB97X–D functionals, respectively. As indicated in Figure 15, similar performances are found for the reduction of 2-chlorocyclohexanol isomers, although in this case M06-2X outperforms M11.

In the presence of EWG, the *trans* isomer is also predicted as the most stable product, while experimental data indicate that the *cis* isomer is obtained as the major compound. However, the stereoselectivity of hydride reductions of cyclohexanones is kinetically controlled and the ratio of reaction products is usually obtained from the Gibbs free energy of the different transition states.[13,19c–e] For the methoxy substituent, the B3LYP–D3 functional (MUE = 0.15 kcal mol^{-1}) reproduces the best the isomer's relative energies, outperforming the Minnesota functionals. However, for the methylthio-substituent, again M06-2X corresponds to the best performing method. As such, the performance of the hybrid functionals for describing the relative stability of the alcohol product also depends on the substituents.

Figure 16 shows the average MUE and RMSD over the entire benchmark set (n = 16) of 2-substituted cyclohexanols (**1**–**4**). From this Figure, it is observed that the overall best performing functionals are the M06 (MUE = 0.31 kcal mol^{-1}) and M06-2X (MUE = 0.35 kcal mol^{-1}, whereas PBE–D3 and MP2 perform the worst. Regarding range-separated hybrid functionals, again ωB97X–D outperforms M11. In contrast to the transition states, single-point energy calculations with B2PLYP–D3 have a negative influence on the performance of the exchange-correlation functionals.

3.5. Overall Performance of DFT Methods for Thermochemistry and Kinetics of Hydride Reductions of Cyclohexanones

Based on the above findings, it becomes clear that the overall performance of the functionals depends on the chemical species along the reaction pathway (reactants, transition states and products) and substituents (Me, OMe, SMe and Cl). As expected, the errors linked to the starting cyclohexanones and alcohol products are much lower as compared to transition states. For the isolated reactants and products, most of the methods agree on the global minima and the statistical errors are in the range of chemical accuracy. For the description of the conformational relative energies of 2-substituted cyclohexanones and cyclohexanols, Minnesota functionals like M06-2X and M06 perform the best, closely followed by B3LYP–D3 and ωB97X–D. However, some of these functionals, specially M06-2X, provides large errors for the description of the transition state energies involved in the hydride reduction of 2-substituted cyclohexanones. This is expected since the reducing

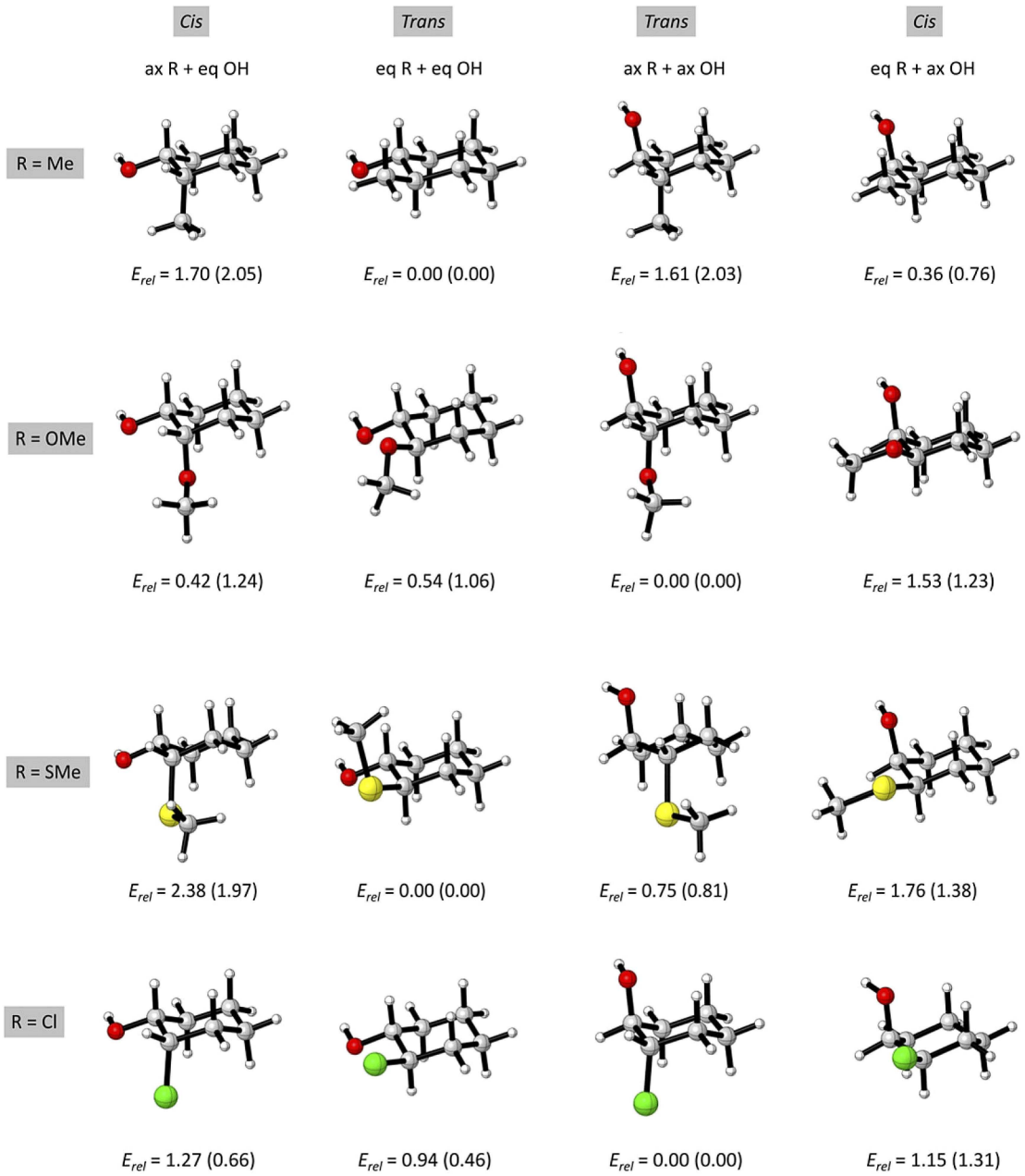

Figure 14. CCSD(T) relative energies for the *cis* and *trans* isomers of the resulting cyclohexanol products (**1**–**4**). The relative energies provided by M06, the best performing functional over this set, are shown in brackets.

agent $LiAlH_4$ is only present in the transition state structures. In view of the importance of the reducing agents in determining the stereoselectivity of the hydride reduction,[3–7] it becomes apparent that the reaction outcome depends mainly on the accurate description of the transition state energies.[19] Therefore, the best performing functional in describing the transition state energies relative to CCSD(T) should be employed for an accurate description of such kinetically-controlled reactions. From Figure 13, it can be inferred that the combination of single-point energy calculations with the double hybrid B2PLYP–D3 functional on ωB97X–D optimized geometries provides the lowest overall MUE (MUE = 0.54 kcal mol^{-1}). Such combined method outperforms the widely used B3LYP–D3 (MUE = 0.73 kcal mol^{-1}) and the standalone ωB97X–D (MUE = 1.09 kcal mol^{-1}). Remarkably, the influence of the optimized geometries on the B2PLYP–D3 energies is rather small as for the CCSD method. On the whole, hybrid density functionals clearly outperforms MP2, which shows the largest deviations from the CCSD(T) reference method.

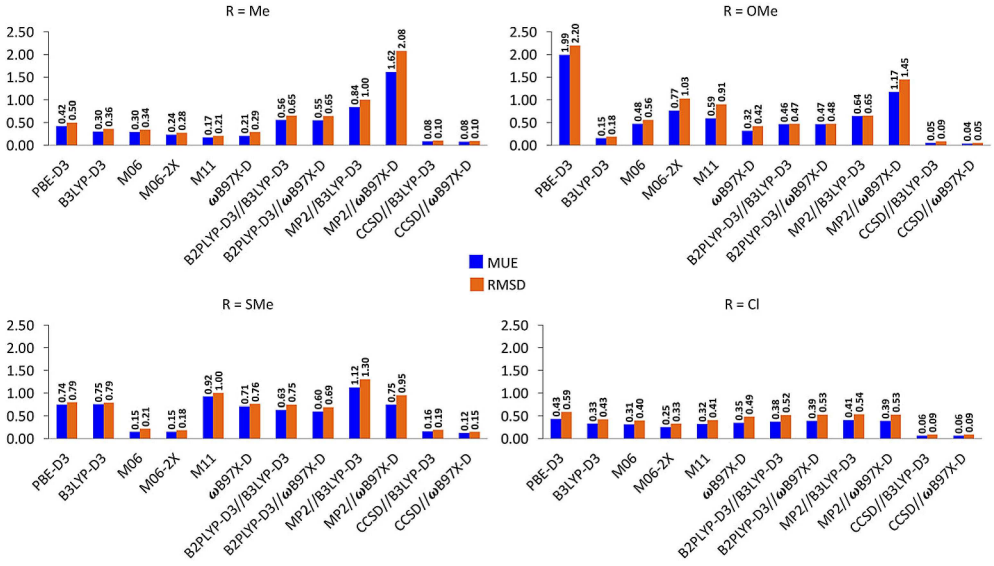

Figure 15. MUE and RMSD (in kcal mol^{-1}) relative to CCSD(T) for describing the relative energies of the different cyclohexanols (**1**–**4**).

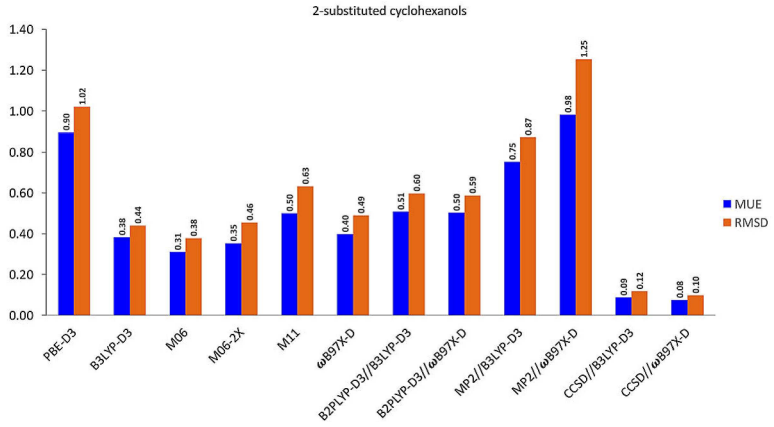

Figure 16. Average MUE and RMSD relative to CCSD(T) for the description of the relative energies of the different cyclohexanols (**1**–**4**) obtained after reduction with $LiAlH_4$.

3.6. Factors Influencing the Stereoselectivity of Hydride Reductions of 2-Substituted Cyclohexanones

Having assessed the performance of different functionals on the description of the $LiAlH_4$ reduction of 2-substituted cyclohexanones, we proceeded with the analysis of the different factors driving the stereoselectivity of such reductions. The B2PLYP–D3/aug-cc-pVTZ//ωB97XD/cc-pVDZ level of theory was selected since it provides transition state energies with the highest accuracy. First, we analysed the influence of the substituent on the conformation of the starting cyclohexanones. Based on Gibbs free energies, 2-methylcyclohexanone preferentially adopts a chair conformation with the methyl group in an equatorial position, whereas those cyclohexanones bearing an EWG substituent (OMe, SMe and Cl) prefers to place the substituent in an axial orientation, in line with the relative energies obtained with the CCSD(T) method. For cyclohexanones **2**–**4**, the equatorial conformation is 0.8-1.3 kcal mol^{-1} higher in energy. As such, the axial conformation stability increased from 2-methyl to 2-chlorocyclohexanone, which is in agreement with reported NMR data and DFT investigations.[56]

To assess the role of noncovalent interactions in the conformational preferences of 2-substituted cyclohexanones, the NCI method was applied.[50] The NCI plots of the axial and equatorial conformations for the different substituents are shown in Figure 17. From the gradient isosurfaces, it becomes clear that the orientation of the substituent induces a significant change on the noncovalent interactions involving the substituent. In the equatorial conformer, the isosurface lies between the substituent and the carbonyl moiety. Such interaction is repulsive closer to the C–C bond and weakly attractive between the heteroatoms. However, the axial conformer is mainly dominated by 1,3-diaxial interactions. Interestingly, the attractive and the repulsive contributions to both interactions are highly dependent on the substituent, as can be inferred from the bidimensional plots of the reduced density

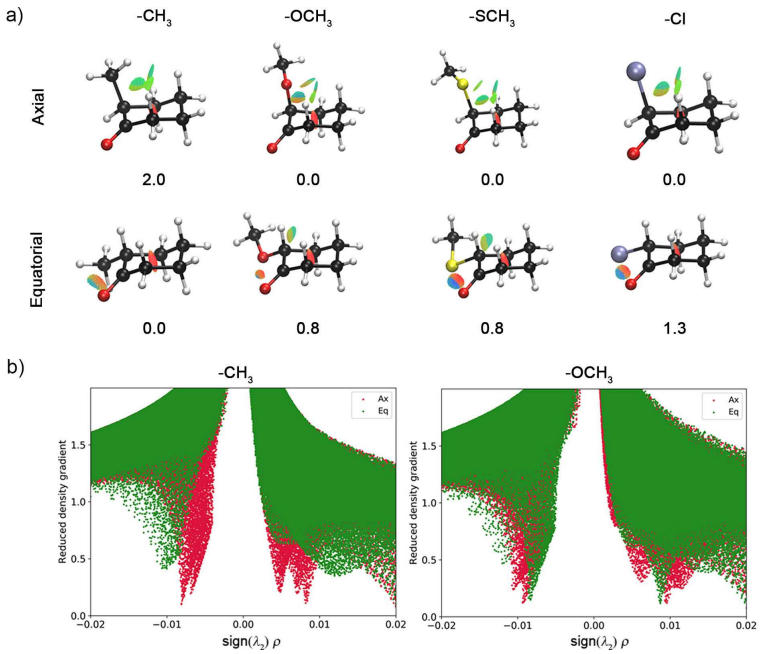

Figure 17. Evolution of the noncovalent interactions in the axial and equatorial conformers of 2-substituted cyclohexanones (**1**-**4**). a) The gradient isosurfaces ($s = 0.5$) are coloured on a RGB scale according to sign(λ_2)ρ over the range −0.02 a.u. to 0.02 a.u. b) Plots of the reduced density gradient *vs* the electron density multiplied by the sign of the second Hessian eigenvalue (λ_2).

gradient *vs* sign(λ_2)ρ (Figure 17b). For the methyl group, the weakening of the interactions when going from the equatorial to the axial conformer is clearly visualized with the shift of the characteristic NCI attractive peaks towards lower density values. In addition, a major repulsive contribution is found for the 1,3-diaxial interactions in the axial conformer, contributing to the large destabilization of this conformer for the methyl substituent. By contrast, for EWG the strength of the attractive peaks is rather similar for both chair conformations, whereas stronger repulsive interactions appear in the equatorial conformer associated to the heteroatom···heteroatom interaction. This repulsive interaction is clearly visualized in the gradient isosurfaces, since red isosurfaces are linked to repulsive interactions. This delicate balance between stabilizing/destabilizing interactions is reflected in the attractive and repulsive contributions to the total integrated value within the NCI region (Table 1). From these values, it is clear that attractive contributions are maximized in the lowest-energy chair conformation for each substituent, whereas the repulsive interactions are minimized.

To assess the substitution effect on the distortion of the six-membered ring, the puckering angle (ϕ), defined as the angle formed by the intersection between the C_2–C_3–C_5–C_6 and C_1–C_2–C_6 planes, was computed for the axial and equatorial conformations. In the equatorial conformers, the puckering angles decreases from 135° in cyclohexanone to 133° in **1** and 131° in **2**–**4**, reducing the flattening of the six-membered ring. However, ϕ_1 increases to 137° upon axial substitution with the methyl group, whereas it decreases for EWG groups. It is noteworthy that the flattening of the cyclohexanone ring is usually associated with increased axial attack.[57]

Table 1. Relative Gibbs free and electronic energies (in kcal mol^{-1}), volume integrations (V_{NCI} in a.u.) within the NCI region and puckering angle (in °) of the axial and equatorial conformations of 2-substituted cyclohexanones.[a]

	CH_3		OCH_3		SCH_3		Cl	
	ax	eq	ax	eq	ax	eq	ax	eq
ΔG_{rel}	2.00	0.00	0.00	0.84	0.00	0.80	0.00	1.18
ΔE_{rel}[b]	1.83	0.00	0.00	1.13	0.00	0.62	0.00	1.34
	(1.87)	(0.00)	(0.00)	(1.78)	(0.00)	(0.33)	(0.00)	(1.35)
D_1[c]	46.9	51.0	58.9	52.6	50.6	53.3	49.1	53.1
ϕ[c]	136.9	133.0	125.5	131.6	133.7	130.9	135.2	131.0
V_{NCI}[d]	2.30	0.62	2.81	0.97	22.61	19.75	8.20	5.31
% attr.	67%	82%	66%	60%	60%	59%	66%	64%
% rep.	33%	18%	34%	40%	40%	41%	34%	36%

[a] Gibss free and electronic energies are calculated at the B2PLYP–D3/aug-cc-pVTZ//ωB97XD/cc-pVDZ level of theory.[b] The electronic energies in parenthesis correspond to the CCSD(T)//cc-pVTZ method.[c] The C_6–C_1–C_2–C_3 dihedral angle (D_1) and the puckering angle (ϕ) in the cyclohexanone ring are 49.1° and 135.5°, respectively. [d] Volume integrations within the NCI region (in a.u.), together with the percentage of attractive and repulsive contributions to the total volume.

The next step involved the evaluation of the relative Gibbs free energies for the eight possible transition structures (Figure 7) for the axial and equatorial additions of $LiAlH_4$ at the selected level of theory. The relative electronic energies, Gibbs free energies of bidentate and tridentate transition states together with the torsional parameters are collected in Table 2. As shown in Figure 18, there is a clear influence of the substituent on the relative stability of the transition states.

For the reduction of 2-methylcyclohexanone (**1**), the lowest-energy transition state corresponds to **TSb** and hence, the axial hydride attack is clearly preferred over the equatorial one (**TSd**). Similar to the starting cyclohexanone, the equatorial conformer of the ketone is more stable than the axial one by 1.5–

Table 2. Relative Gibbs free and electronic energies (in kcal mol^{-1}) together with selected torsional parameters (in °) of the bi- and tri-dentate transition states involved in the $LiAlH_4$ reduction of 2-substituted cyclohexanones.[a]

CH_3	a	b	c	d	a′	b′	c′	d′
ΔG_{THF}[b]	1.61	0.00	3.91	1.41	3.99	2.36	5.37	3.78
ΔG_{rel}	1.58	0.00	3.89	1.79	2.87	1.41	4.36	2.59
ΔE_{rel}[c]	1.89	0.42	4.12	1.89	1.64	0.00	3.36	1.11
	(3.18)	*(1.50)*	*(5.01)*	*(2.84)*	*(1.58)*	*(0.00)*	*(3.08)*	*(0.89)*
D_1[d]	39.8	40.5	61.8	61.5	40.9	41.8	61.9	61.3
ϕ_1[d]	143.8	143.3	121.3	122.4	142.8	142.1	121.2	122.5
D_2[d]	41.1	41.7	36.8	35.6	44.1	43.8	39.2	39.2
OCH_3	a	b	c	d	a′	b′	c′	d′
ΔG_{THF}[b]	9.64	0.12	11.37	0.00	11.95	10.21	11.80	0.00
ΔG_{rel}	8.14	0.34	9.53	0.00	9.50	8.26	9.09	0.00
ΔE_{rel}[c]	11.12	0.44	11.29	0.00	10.51	9.07	9.95	0.00
	(12.08)	*(0.75)*	*(11.69)*	*(0.00)*	*(10.09)*	*(9.13)*	*(9.30)*	*(0.00)*
D_1[d]	40.0	41.2	65.2	61.4	42.2	40.7	64.8	61.4
ϕ_1[d]	142.6	143.2	118.7	123.2	142.0	143.3	119.2	123.2
D_2[d]	39.2	40.0	37.4	33.5	42.9	41.8	39.0	33.5
SCH_3	a	b	c	d	a′	b′	c′	d′
ΔG_{THF}[b]	4.95	0.55	9.01	0.00	7.01	6.76	9.33	7.36
ΔG_{rel}	3.97	0.09	8.62	0.00	5.08	3.97	8.19	7.06
ΔE_{rel}[c]	5.51	0.18	9.27	0.00	5.16	6.14	7.97	7.46
	(5.74)	*(0.00)*	*(9.09)*	*(0.04)*	*(4.16)*	*(5.72)*	*(6.88)*	*(6.71)*
D_1[d]	40.8	41.9	62.5	62.9	41.9	41.6	62.7	60.7
ϕ_1[d]	143.1	142.5	120.9	121.4	142.1	142.5	120.6	123.3
D_2[d]	40.4	40.2	37.1	34.9	42.8	41.9	39.0	36.8
Cl	a	b	c	d	a′	b′	c′	d′
ΔG_{THF}[b]	_[e]	0.03	7.24	0.00	5.43	_[e]	7.08	_[e]
ΔG_{rel}	_[e]	0.00	7.35	0.80	4.28	_[e]	6.28	_[e]
ΔE_{rel}[c]	_[e]	0.00	7.29	1.04	3.28	_[e]	5.13	_[e]
	_[e]	*(0.00)*	*(7.29)*	*(1.05)*	*(2.51)*	_[e]	*(4.30)*	_[e]
D_1[d]	_[e]	41.4	62.3	63.3	37.9	_[e]	62.8	_[e]
ϕ_1[d]	_[e]	143.4	121.4	121.8	146.1	_[e]	120.9	_[e]
D_2[d]	_[e]	38.9	35.9	31.4	42.8	_[e]	37.1	_[e]

[a] Gibbs free energies in gas-phase and solvent together with the electronic energies computed at the [SMD(THF)]/B2PLYP–D3/aug-cc-pVTZ//ωB97XD/cc-pVDZ level of theory. [b] ΔG_{THF} in THF at −78 °C.[c] The electronic energies in parenthesis correspond to the CCSD(T)/ cc-pVTZ method.[d] The C_6–C_1–C_2–C_3 and the O–C_1–C_6–H_{eq} dihedral angles (D_1 and D_2) and the puckering angle (ϕ) in the cyclohexanone ring are 49.1°, 6.6° and 135.5°, respectively.[e] These transition structures converged to a different transition structure.

2.1 kcal mol^{-1}, benefiting from the mitigation of 1,3-diaxial interactions. The predicted ratio of *cis*:*trans* alcohols considering all feasible pathways is 11:89 at 25 °C (or 4:96 at −78 °C), which is in excellent agreement with the experimental ratio at −78 °C of 11:89 (Figure 4). Both **TSb** and **TSb'** led to the formation of the *trans* alcohol bearing both the OH and the CH_3 groups in an equatorial position. This *trans* alcohol is *ca.* 1 kcal mol^{-1} lower in energy than the *cis* alcohol obtained from **TSd** (Table S4). Accordingly, the axial addition to cyclohexanone **1** is clearly favoured from the kinetic and thermodynamic point of view, consistent with the experimental observations.

A different stereoselectivity is, however, found for the reduction of cyclohexanones **2–4** bearing an electron-withdrawing substituent. According to Figure 18, the pathway involving the bidentate **TSd** becomes favoured under kinetic control conditions, closely followed by **TSb**. Interestingly, both transition states adopt an equatorial conformation for the ketone in the presence of the $LiAlH_4$, which is due to the additional coordination of the counterion Li^+ with the heteroatom. Such double coordination is not possible for **TSa** and **TSc** and its tridentate analogues, bearing the substituent in an axial conformation (Figure 19). As such, these transition structures are largely destabilized in the reduction of **2–4**. The NCI analysis shows indeed strong and directional interactions involving the counterion and the heteroatom of the OMe, SMe and Cl, but only in the equatorial orientation (Figure S2).

Regarding the facial selectivity for the hydride attack, small Gibbs free energy differences between **TSb** and **TSd** are computed, corresponding to the axial and equatorial attack, respectively. For the OMe, a 78:22 ratio of *cis*:*trans* alcohols at 25 °C (or 73:27 at −78 °C in THF) is estimated, indicating an equatorial preference for the addition of the $LiAlH_4$. Unfortunately, the NMR-spectra of the resulting 2-methoxycyclohexanol was unsuitable to extract fiable experimental data. In the case of the SMe, **TSd** remains the most stable transition structure and accordingly, the $LiAlH_4$ prefer to add to the equatorial face of the cyclohexanone, yielding the *cis* alcohol. A 54:46 ratio of *cis*:*trans* alcohols is estimated for the gas-phase at room temperature, but the reduction reaction becomes more stereoselective at −78 °C in THF with a 81:19 ratio, in excellent agreement with the experimental ratio of 79:21. It is interesting to note that the competing **TSb**, corresponding to an axial

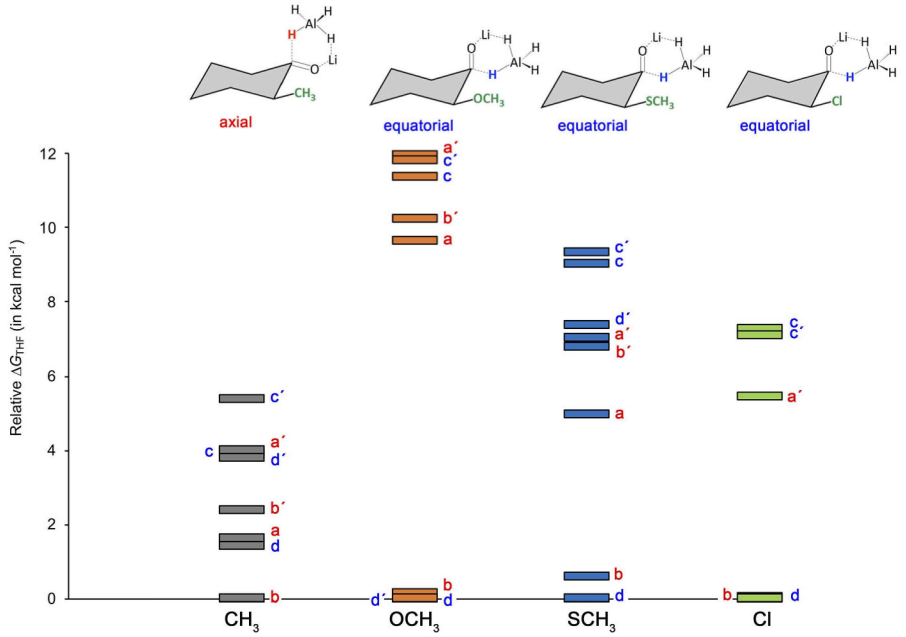

Figure 18. Relative Gibbs free energies in THF and −78 °C of the bi- and tridentate transition structures for axial (red) and equatorial (blue) hydride additions to 2-substituted cyclohexanones.

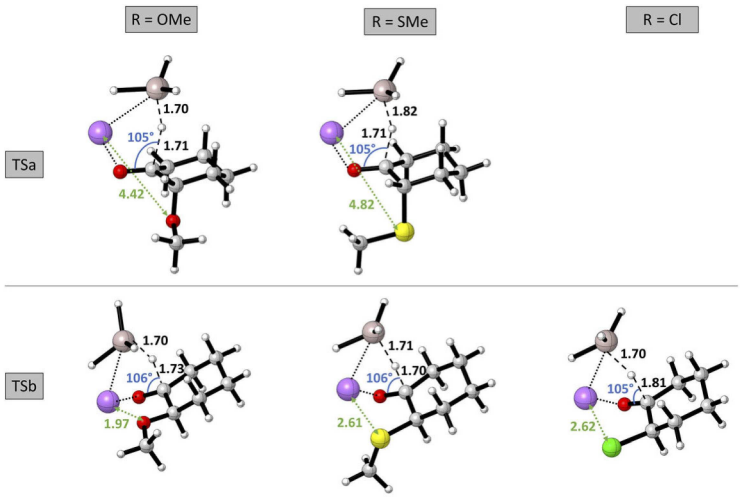

Figure 19. Different coordination of the Li^+ counterion in the TSs of the axial hydride attack to 2-substituted cyclohexanones with the electron-withdrawing group in axial and equatorial position, respectively.

attack of the hydride, becomes destabilized upon solvation corrections and low temperature (Table 2). The prediction of the stereoselectivity of the reduction of 2-chlorocyclohexanone is more challenging. Whereas **TSb** is more stable than **TSd** in gas phase ($\Delta G = 0.8$ kcal mol^{-1}), **TSd** becomes slightly favoured under kinetic control conditions. **TSb** involves a hydride axial attack preferentially yielding the *trans* alcohol, whereas **TSd** correspond to an equatorial attack leading to a predominant *cis* alcohol in line with the experimental ratio. As such, from the computed energies the reduction of **4** with $LiAlH_4$ is predicted to be not highly stereoselective.

Having identified the preferred transition states for the differently-substituted cyclohexanones (**1**–**4**), we assess if the torsional strain is the factor governing the stability of the transition structures, as stated by the Felkin-Anh model.[8] The analysis of the dihedral angle D_2(O–C_1–C_6–H_{eq}) indicates that the torsional strain is reduced in the transition states corresponding to the axial hydride addition. An increase in D_2 is linked to a decrease in the torsional strain in the TS, as the carbonyl bond and the neighbouring C–H_{eq} bond becomes less eclipsed (Figure 20). From Table 2, it is clear that D_2 is larger for the bi- and tridentate transition states involving an axial hydride addition (**TSa**, **TSb**, **TSa'** and **TSb'**), irrespective of the substituent.

On the other side, D_1(C_6–C_1–C_2–C_3) and ϕ_1 measure the deformation of the cyclohexanone ring. An increase in D_1

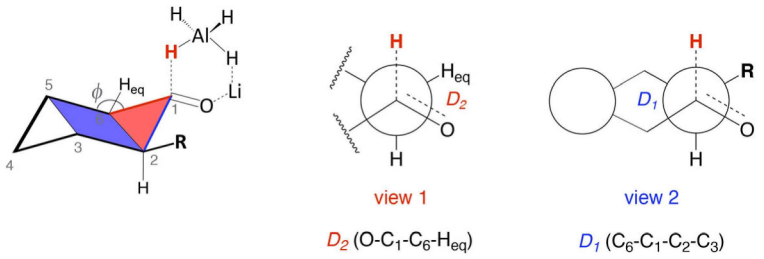

Figure 20. Measurement of the torsional strain in the TS of hydride addition to cyclohexanones.

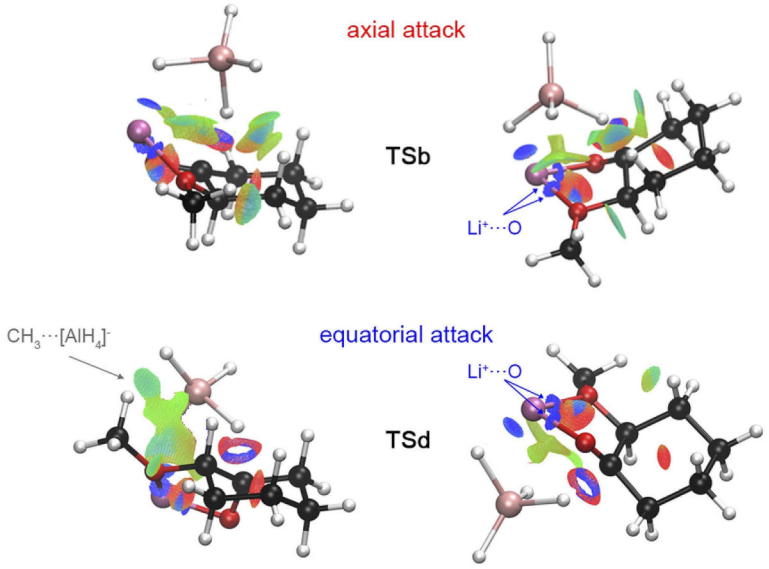

Figure 21. NCI analysis of the interactions in the transition structures corresponding to an axial and equatorial hydride attack to 2-methoxycyclohexanone **2**. The gradient isosurfaces ($s = 0.5$) are coloured on a RGB scale according to sign(λ_2)ρ over the range −0.02 a.u. to 0.02 a.u.

indicates an enhanced torsional strain,[19d] while the six-membered ring becomes more puckered. In line with previous analysis, D_1 increases by ca. 20° in the TSs corresponding to an equatorial hydride attack (**TSc**, **TSd**, **TSc'** and **TSd'**) as compared to the axial transition structures (**TSa**, **TSb**, **TSa'** and **TSb'**) for all substituents. Therefore, according to the torsional strain of the TSs, axial hydride attack is predicted to be favoured regardless of the substituent.

Since the relative Gibbs free energies indicate a subtle preference for the equatorial attack in the presence of electron-withdrawing substituents, the stereoselectivity in the reduction reactions is clearly governed by other factors. The NCI analysis show the different noncovalent interactions present in **TSb** and **TSd** (Figure 21). Both transition structures exhibit strong attractive interactions involving the Li^+ and the carbonyl group and the OMe group. In this case, the complexation with the counterion seems not to be responsible for facial stereoselectivity as very similar Li^+···O and Li^+···OMe strengths are computed for **TSb** and **TSd**. It is noteworthy that the dispersion interactions between AlH_4^- and OMe is more delocalized in **TSd** as compared to **TSb**, due to its proximity.

In addition, the energetic profiles for the two competing pathways of the reduction of 2-methoxycyclohexanone by $LiAlH_4$ (Figure 22) indicates that the pre-reactive coordination complex for the equatorial addition is favoured over the axial

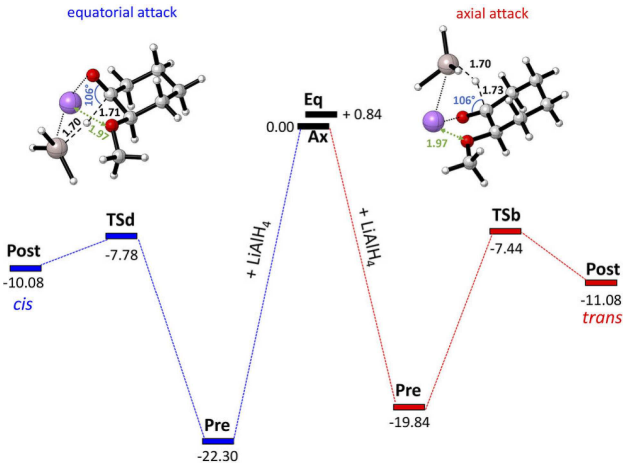

Figure 22. Gibbs free energies profiles (in kcal mol^{-1}) for the two competing pathways of the reduction of 2-methoxycyclohexanone by $LiAlH_4$.

addition by 2.5 kcal mol^{-1}. Altogether, our findings point out that the stereoselectivity of the reduction of 2-methylcyclohexanone is dominated by the torsional strain favoring the axial addition, whereas for electron-withdrawing substituents the delicate interplay between torsional strain and dispersion interactions favours the addition to the equatorial face.

4. Conclusion

In order to assess the effect of different parameters on the facial selectivity of hydride reductions of 2-substituted cyclohexanones, a thorough benchmark study involving DFT and wave-function methods was first performed. From this benchmark, we found that the performance of the functionals strongly depends on the chemical species along the reaction pathway (reactants, transition states and products) and substituents (Me, OMe, SMe and Cl). As expected, the errors linked to the starting cyclohexanones and alcohol products are much lower as compared to transition states. For the isolated reactants and products, most of the methods agree on the global minima and the errors are in the range of chemical accuracy. Minnesota functionals like M06-2X and M06, closely followed by B3LYP–D3 and ωB97X–D, seem to deliver relative energies of 2-substituted cyclohexanones and cyclohexanols in close agreement with the CCSD(T) reference data. Nevertheless, since the facial stereoselectivity is determined by the transition state structures, the best performing functional in describing the transition states energies relative to CCSD(T) should be employed for an accurate description of such kinetically-controlled reactions. In this regard, double hybrid functionals appear to be the best option. An overall MUE of 0.54 kcal mol^{-1} is obtained when single-point energy calculations are performed with the B2PLYP–D3 functional on ωB97X–D optimized geometries. This combined methodology was subsequently used to describe the role of torsional strain, complexation and non-covalent interactions on the stereoselectivity. Importantly, the experimental *cis:trans* ratios are well reproduced by the computational data.

The facial selectivity of $LiAlH_4$ reduction strongly depends on the substituent. Whereas for the 2-methylcyclohexanone an axial attack is driven by the lowering of the torsional strain, the equatorial attack seems to be preferred in the presence of electron-withdrawing groups. In this case, a delicate interplay between complexation, torsional strain and dispersion interactions favours the addition to the equatorial face. Overall, the Felkin-Ahn model appears to be insufficient to predict the facial selectivity of the hydride addition to 2-substituted cyclohexanones.

Experimental Section

The reduction of 2-substituted cyclohexanones towards the respective 2-substituted cyclohexanols with $LiAlH_4$ as the reducing agent is well described in literature, which facilitated the acquisition of experimental data.[24] Diastereoisomer ratios were determined by ^{1}H-NMR spectra of the crude reaction mixture using the integration of the proton at C_1. A detailed description concerning the synthetic procedure and determination of the *cis:trans* ratios can be found in the Supporting Information.

Acknowledgements

The authors wish to thank the Fund for Scientific Research – Flanders (FWO) and the Vrije Universiteit Brussel (VUB) for their continuous support. F.D.P. acknowledges the VUB for a Strategic Research Program and also acknowledges the Francqui Foundation for a position as Francqui research professor. M. A. thanks the FWO for a postdoctoral fellowship (12F4416 N) and the VUB for financial support. R.V.L. thanks Karel Duerincx (KU Leuven) for the assistance with NMR measurements and acknowledges the FWO for a predoctoral fellowship. Computational resources and services were provided by the Shared ICT Services Centre funded by the Vrije Universiteit Brussel, the Flemish Supercomputer Center (VSC) and FWO. The graphical representations of the geometries were obtained using the freely available CYLview[58] software.

Conflict of Interest

The authors declare no conflict of interest.

Keywords: benchmark · density functional calculations · hydride reduction · quantum chemistry · stereochemistry

[1] J. Clayden, N. Greeves, S. Warren, *Org. Chem., Oxford University Press, 2nd edition*, **2012**, p. 1260.
[2] E. Juaristi, *Conformational Behavior of Six-Membered Rings: Analysis, Dynamics and Stereoelectronic Effects*, Wiley-VCH, Weinheim, **1995**, p. 306.
[3] J. Seyden-Penne, *Reductions by the Alumino- and Borohydrides in Organic Synthesis, Wiley-VCH, Weinheim, 2nd edition*, **1997**, p. 224.
[4] J. L. Pierre, H. Handel, R. Perraud, *Tetrahedron* **1975**, *31*, 2795.
[5] H. Handel, J. L. Pierre, *Tetrahedron* **1975**, *31*, 2799.
[6] J. Durand, N. Trong Anh, J. Huet, *Tetrahedron Lett.* **1974**, *15*, 2397.
[7] B. Rickborn, M. T. Wuesthoff, *J. Am. Chem. Soc.* **1970**, *92*, 6894.
[8] a) M. Chérest, H. Felkin, N. Prudent, *Tetrahedron Lett.* **1968**, *18*, 2199; b) M. Chérest, H. Felkin, N. Prudent, *Tetrahedron Lett.* **1968**, *18*, 2205; c) A. Mengel, O. Reiser, *Chem. Rev.* **1999**, *99*, 1191.
[9] H. B. Bürgi, J. D. Dunitz, J. M. Lehn, G. Wipff, *Tetrahedron* **1974**, *30*, 1563.
[10] J. Klein, *Tetrahedron Lett.* **1973**, *44*, 4307.
[11] Y.-D. Wu, J. A. Tucker, K. N. Houk, *J. Am. Chem. Soc.* **1991**, *113*, 5018.
[12] A. S. Cieplak, *J. Am. Chem. Soc.* **1981**, *103*, 4540.
[13] S. R. Neufeldt, G. Jiménez-Osés, D. L. Comins, K. N. Houk, *J. Org. Chem.* **2014**, *79*, 11609.
[14] W. C. Dauben, G. J. Fonken, D. S. Noyce, *J. Am. Chem. Soc.* **1956**, *78*, 2579.
[15] G. Frenking, K. F. Köhler, M. T. Reetz, *Angew. Chem.* **1991**, *103*, 1166; *Angew. Chem. Int. Ed.* **1991**, *30*, 1146.
[16] a) R. R. Fraser, M. Stanciulescu, *J. Am. Chem. Soc.* **1987**, *109*, 1580; b) R. P. Kirchen, K. Ranganayakulu, T. S. Sorensen, *J. Am. Chem. Soc.* **1987**, *109*, 7811; c) T. Laube, H. U. Stilz, *J. Am. Chem. Soc.* **1987**, *109*, 5876.
[17] a) S. Danishefsky, M. E. Langer, *J. Org. Chem.* **1985**, *50*, 3674; b) A. S. Cieplak, B. Tait, C. R. Johnson, *J. Am. Chem. Soc.* **1985**, *111*, 8447; c) C. K. Cheung, L. T. Tseng, M.-H. Lin, S. Srivastava, W. J. le Noble, *J. Am. Chem. Soc.* **1986**, *108*, 1598; d) H. Li, W. J. le Noble, *Tetrahedron Lett.* **1990**, *31*, 4391; e) G. Mehta, F. A. Khan, *J. Am. Chem. Soc.* **1990**, *112*, 6140; f) J. M. Hahn, W. J. le Noble, *J. Am. Chem. Soc.* **1992**, *114*, 1916; g) B. Ganguly, J. Chandrasekhar, F. A. Khan, G. Metha, *J. Org. Chem.* **1993**, *58*, 1734; h) Y. Senda, S. Nakano, H. Kunii, H. Itoh, *J. Chem. Soc. Perkin Trans.* **1993**, *2*, 1009.

[18] a) E. P. Lodge, C. H. Heathcock, *J. Am. Chem. Soc.* **1987**, *109*, 3353; b) Y.-D. Wu, K. N. Houk, *J. Am. Chem. Soc.* **1987**, *109*, 908; c) D. Mukherjee, Y.-D. Wu, F. R. Fronckzek, K. N. Houk, *J. Am. Chem. Soc.* **1988**, *110*, 3328; d) A. I. Meyers, M. A. Sturgess, *Tetrahedron Lett.* **1988**, *29*, 5339; e) A. I. Meyers, R. H. Wallace, *J. Org. Chem.* **1989**, *54*, 2509; f) R. E. Rosenberg, R. L. Abel, M. D. Drake, D. J. Fox, A. K. Ignatz, D. M. Kwiat, K. M. Schaal, P. R. Virkler, *J. Org. Chem.* **2001**, *66*, 1694; g) D. Kaneno, S. Tomoda, *Tetrahedron Lett.* **2004**, *45*, 4559.

[19] a) Y.-D. Wu, K. N. Houk, M. N Paddon-Row, *Angew. Chem.* **1992**, *104*, 1087; *Angew. Chem. Int. Ed.* **1992**, *31*, 1019; b) K. Ando, K. N. Houk, J. Busch, A. Menassé, U. Séquin, *J. Org. Chem.* **1998**, *63*, 1761; c) R. T. Luibrand, I. R. Taigounov, A. A. Taigounov, *J. Org. Chem.* **2001**, *66*, 7254; d) C. C. Bocca, E. A. Basso, G. F. Gauze, *Chem. Phys. Lett.* **2005**, *413*, 434; e) C. C. Bocca, R. Rittner, A. P. da Silva, E. A. Basso, *J. Phys. Org. Chem.* **2011**, *24*, 241.

[20] a) C. Lee, W. Yang, R. G. Parr, *Phys. Rev. B* **1988**, *37*,785; b) A. D. Becke, *J. Chem. Phys.* **1993**, *98*, 1372.

[21] a) Y. Zhao, D. G. Truhlar, *Theor. Chem. Acc.* **2008**, *120*, 215; b) Y. Zhao, D. G. Truhlar, *J. Chem. Theory Comput.* **2008**, *4*, 1849; c) Y. Zhao, D. G. Truhlar, *Chem. Phys. Lett.* **2011**, *502*, 1; d) R. Peverati, D. G. Truhlar, *Phys. Chem. Chem. Phys.* **2012**, *14*, 11363; e) R. Peverati, D. G. Truhlar, *Phil. Trans. R. Soc. A* **2014**, *372*, 20120476; f) X. Li, X. Xu, X. You, D. G. Truhlar, *J. Phys. Chem. A* **2016**, *120*, 4025; g) N. Mardirossian, M. Head-Gordon, *J. Chem. Theory Comput.* **2016**, *12*, 4303; h) A. T. Pereira, A. J. M. Ribeiro, P. A. Fernandes, M. J. Ramos, *Int. J. Quantum Chem.* **2017**, *117*, e25409.

[22] a) P. Hao, J. Sun, B. Xiao, A. Ruzsinszky, G. I. Csonka, J. Tao, S. Glindmeyer, J. P. Perdew, *J. Chem. Theory Comput.* **2013**, *9*, 355; b) B. Chan, A. T. B. Gilbert, P. M. W. Gill, L. Radom, *J. Chem. Theory Comput.* **2014**, *10*, 3777; c) L.-J. Yu, F. Sarrami, R. J. O'Reilly, A. Karton, *Mol. Phys.* **2015**, *114*, 21; d) L. Goerigk, A. Hansen, C. Bauer, S. Ehrlich, A. Najibi, S. Grimme, *Phys. Chem. Chem. Phys.* **2017**, *19*, 32184; e) M. Torrent-Sucarrat, S. Navarro, F. P. Cossio, J. M. Anglada, J. M. Luis, *J. Comput. Chem.* **2017**, *38*, 2819; f) S. Dohm, A. Hansen, M. Steinmetz, S. Grimme, M. P. Checinski, *J. Chem. Theory Comput.* **2018**, *14*, 2596.

[23] a) l. Ying Zhang, J. Wu, X. Xu, *Chem. Commun.* **2010**, *46*, 3057; b) L. Goerigk, S. Grimme, *Phys. Chem. Chem. Phys.* **2011**, *13*, 6670; c) H. Kruse, L. Goerigk, S. Grimme, *J. Org. Chem.* **2012**, *77*, 10824; d) C. Ehm, P. H. M. Budzelaar, V. Busico, *J. Organomet. Chem.* **2015**, *775*, 39; e) D. Coskun, S. V. Jerome, R. A. Friesner, *J. Chem. Theory Comput.* **2016**, *12*, 1121; f) N. Q. Su, X. Xu, *Annu. Rev. Phys. Chem.* **2017**, *68*, 155.

[24] a) H. C. Brown, H. R. Deck, *J. Am. Chem. Soc.* **1965**, *87*, 5620; b) N. B. Malkar, V. G. Kumar, *Synth. Commun.* **1998**, *28*, 977; c) M. C. Carreno, E. Dominguez, J. L. Garcia-Ruano, A. Rubio, *J. Org. Chem.* **1987**, *52*, 3619; d) G.-D. Roiban, R. Agudo, M. T. Reetz, *Angew. Chem. Int. Ed.* **2014**, *53*, 8659; e) O. O. Kolodiazhna, A. O. Kolodiazhna, O. I. Kolodiazhnyi, *Tetrahedron: Asymmetry* **2013**, *24*, 37.

[25] J. D. Chai, M. Head-Gordon, *Phys. Chem. Chem. Phys.* **2008**, *10*, 6615.

[26] a) Y. Minenkov, A. Singstad, G. Occhipinti, V. R. Jensen, *Dalton Trans.* **2012**, *41*, 5526; b) G. F. Mangiatordi, E. Brémond, C. Adamo, *J. Chem. Theory Comput.* **2012**, *8*, 3082; c) M. L. Laury, A. K. Wilson, *J. Chem. Theory Comput.* **2013**, *9*, 3939; d) E. Brémond, M. Savarese, N. Q. Su, A. J. Pérez-Jiménez, X. Xu, J. C. Sancho-Garcia, C. Adamo, *J. Chem. Theory Comput.* **2016**, *12*, 459; e) R. K. Raju, A. A. Bengali, E. N. Brothers, *Dalton Trans.* **2016**, *45*, 13766; f) N. Mardirossian, M. Head-Gordon, *Mol. Phys.* **2017**, *115*, 2315; g) Y. Minenkov, H. Wang, Z. D. Wang, S. M. Sarathy, L. Cavallo, *J. Chem. Theory Comput.* **2017**, *13*, 3537; h) N. Kosar, T. Mahmood, K. Ayub, *J. Mol. Struct.* **2017**, *1150*, 447; i) S. Zaczek, F. Gelman, A. Dybala-Defratyka, *J. Phys. Chem. A* **2017**, *121*, 2311; j) B. Dash, *Comput. Theor. Chem.* **2018**, *1128*, 1.

[27] a) S. Grimme, *J. Chem. Phys.* **2006**, *124*, 034108; b) L. Goerigk, S. Grimme, *WIREs Comput. Mol. Sci.* **2014**, *4*, 576.

[28] C. Møller, M. S. Plesset, *Phys. Rev.* **1934**, *46*, 618.

[29] K. Raghavachari, G. W. Trucks, J. A. Pople, M. Head-Gordon, *Chem. Phys. Lett.* **1989**, *157*, 479.

[30] J. P. Perdew, K. Schmidt, *AIP Conf. Proc.* **2001**, *577*, 1.

[31] W. Kohn, L. J. Sham, *Phys. Rev.* **1965**, *140*, A1133.

[32] P. W. Ayers, R. G. Parr, *Int. J. Quantum Chem.* **2003**, *95*, 877.

[33] M. M. Morrell, R. G. Parr, M. Levy, *J. Chem. Phys.* **1975**, *62*, 549.

[34] J. P. Perdew, *Phys. Rev. Lett.* **1985**, *55*, 1665.

[35] J. P. Perdew, K. Burke, M. Ernzerhof, *Phys. Rev. Lett.* **1996**, *77*, 3865.

[36] J. P. Perdew, K. Burke, M. Ernzerhof, *Phys. Rev. Lett.* **1997**, *78*, 1396.

[37] J. P. Perdew, K. Burke, M. Ernzerhof, *Phys. Rev. B* **1986**, *33*, 8822.

[38] T. Van Voorhis, G. E. Scuseria, *J. Chem. Phys.* **1998**, *109*, 400.

[39] E. I. Proynov, E. Ruiz, A. Vela, D. R. Salahub, *Int. J. Quantum Chem.* **1995**, *29*, 61.

[40] R. Peveratti, D. G. Truhlar, *J. Phys. Chem. Lett.* **2001**, *2*, 2810.

[41] Gaussian Revision **D01**, M. J. Frisch, G. W. Trucks, H. B. Schlegel, G. E. Scuseria, M. A. Robb, J. R. Cheeseman, G. Scalmani, V. Barone, G. A. Petersson, H. Nakatsuji, X. Li, M. Caricato, A. Marenich, J. Bloino, B. G. Janesko, R. Gomperts, B. Mennucci, H. P. Hratchian, J. V. Ortiz, A. F. Izmaylov, J. L. Sonnenberg, D. Williams-Young, F. Ding, F. Lipparini, F. Egidi, J. Goings, B. Peng, A. Petrone, T. Henderson, D. Ranasinghe, V. G. Zakrzewski, J. Gao, N. Rega, G. Zheng, W. Liang, M. Hada, M. Ehara, K. Toyota, R. Fukuda, J. Hasegawa, M. Ishida, T. Nakajima, Y. Honda, O. Kitao, H. Nakai, T. Vreven, K. Throssell, J. A. Montgomery, Jr., J. E. Peralta, F. Ogliaro, M. Bearpark, J. J. Heyd, E. Brothers, K. N. Kudin, V. N. Staroverov, T. Keith, R. Kobayashi, J. Normand, K. Raghavachari, A. Rendell, J. C. Burant, S. S. Iyengar, J. Tomasi, M. Cossi, J. M. Millam, M. Klene, C. Adamo, R. Cammi, J. W. Ochterski, R. L. Martin, K. Morokuma, O. Farkas, J. B. Foresman, and D. J. Fox, Gaussian, Inc., Wallingford CT, **2016**.

[42] T. H. Dunning, *J. Chem. Phys.* **1989**, *90*, 1007.

[43] a) S. Grimme, J. Antony, S. Ehrlich, H. Krieg, *J. Chem. Phys.* **2010**, *132*, 154104; b) S. Grimme, S. Ehrlich, L. Goerigk, *J. Comput. Chem.* **2011**, *32*, 1456.

[44] R. A. Kendall, T. H. Dunning, R. J. Harrison, *J. Chem. Phys.* **1992**, *96*, 6796.

[45] S. E. Wheeler, K. N. Houk, *J. Chem. Theory Comput.* **2010**, *6*, 395.

[46] a) G. D. Purvis, R. J. Bartlett, *J. Chem. Phys.* **1982**, *76*, 1910; b) G. E. Scuseria, C. L. Janssen, H. F. Schaefer, *J. Chem. Phys.* **1988**, *89*, 7382; c) G. E. Scuseria, H. F. Schaefer, *J. Chem. Phys.* **1989**, *90*, 3700.

[47] MOLPRO, version 2012.1, a package of ab initio programs, H.-J. Werner, P. J. Knowles, G. Knizia, F. R. Manby, M. Schütz, P. Celani, T. Korona, R. Lindh, A. Mitrushenkov, G. Rauhut, K. R. Shamasundar, T. B. Adler, R. D. Amos, A. Bernhardsson, A. Berning, D. L. Cooper, M. J. O. Deegan, A. J. Dobbyn, F. Eckert, E. Goll, C. Hampel, A. Hesselmann, G. Hetzer, T. Hrenar, G. Jansen, C. Köppl, Y. Liu, A. W. Lloyd, R. A. Mata, A. J. May, S. J. McNicholas, W. Meyer, M. E. Mura, A. Nicklass, D. P. O'Neill, P. Palmieri, D. Peng, K. Pflüger, R. Pitzer, M. Reiher, T. Shiozaki, H. Stoll, A. J. Stone, R. Tarroni, T. Thorsteinsson, and M. Wang.

[48] A. V. Marenich, C. J. Cramer, D. G. Truhlar *J. Phys. Chem. B* **2009**, *113*, 6378.

[49] J. Contreras-Garcia, E. R. Johnson, S. Keinan, R. Chaudret, J.-P. Piquemal, D. N. Beratan, W. Yang, *J. Chem. Theory Comput.* **2011**, *7*, 625.

[50] E. R. Johnson, S. Keinan, P. Mori-Sanchez, J. Contreras-Garcia, A. J. Cohen, W. Yang, *J. Am. Chem. Soc.* **2010**, *132*, 6498.

[51] a) J. Contreras-Garcia, W. Yang, E. R. Johnson, *J. Phys. Chem. A* **2011**, *115*, 12983; b) M. Alonso, T. Woller, F. J. Martin-Martinez, J. Contreras-Garcia, P. Geerlings, F. De Proft, *Chem. Eur. J.* **2014**, *20*, 4931.

[52] W. Humphrey, A. Dalke, K. Schulten, *J. Mol. Graphics* **1996**, *14*, 33.

[53] J. Contreras-Garcia, R. A. Boto, F. Izquierdo-Ruiz, I. Reva, T. Woller, M. Alonso, *Theor. Chem. Acc.* **2016**, *135*, 242.

[54] R. Peverati, D. G. Truhlar, *J. Phys. Chem. Lett.* **2012**, *3*, 117.

[55] a) S. Kozuch, J. M. L. Martin, *Phys. Chem. Chem. Phys.* **2011**, *13*, 20104; b) S. Kozuch, J. M. L. Martin, *J. Comb. Chem.* **2013**, *34*, 2327.

[56] a) E. A. Basso, C. Kaiser, R. Rittner, J. B. Lambert, *J. Org. Chem.* **1993**, *58*, 7865; b) F. Yoshinaga, C. F. Tormena, M. P. Freitas, R. Rittner, R. J. Abraham, *J. Chem. Soc.* **2002**, *2*, 1494; c) M. P. Freitas, C. F. Tormena, J. C. Garcia, R. Rittner, R. J. Abraham, E. A. Basso, F. P. Santos, J. C. Cedran, *J. Phys. Org. Chem.* **2003**, *16*, 833; d) F. Azarakhshi, D. Nori-Shargh, H. Attar, N. Masnabadi, H. Yahyaei, S. N. Mousavi, J. E. Boggs, *Mol. Simul.* **2011**, *37*, 1207.

[57] a) W. T. Wipke, P. Gund, *J. Am. Chem. Soc.* **1976**, *98*, 8107; b) J. M. Coxon, K. N. Houk, R. T. Luibrand, *J. Org. Chem.* **1995**, *60*, 418.

[58] CYLview, 1.0b, C. Y. Legault, Université de Sherbrooke, **2009**.

Manuscript received: March 6, 2019
Revised manuscript received: May 10, 2019